Journal of Computational Physics 551 (2026) 114671

Contents lists available at ScienceDirect

Journal of Computational Physics

journal homepage: www.elsevier.com/locate/jcp

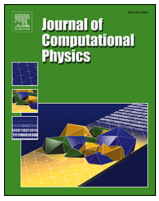

On ground states of spin-1 dipolar Bose-Einstein condensate: Dimension reduction and numerical computation

Zhixuan Li [a], Qinglin Tang [a], Hanquan Wang [b], Yong Zhang [c,*]

[a] School of Mathematics, Sichuan University, 610064, Chengdu, China
[b] School of Statistics and Mathematics, Yunnan University of Finance and Economics, 650221, Kunming, China
[c] Center for Applied Mathematics and KL-AAGDM, Tianjin University, 300072, Tianjin, China

ARTICLE INFO

Keywords:
Gross-Pitaevskii equations
Spin-1 dipolar BEC
Dimension reduction
Ground state
Projected gradient flow
Kernel truncation method

ABSTRACT

We perform a dimension reduction for spin-1 dipolar Bose-Einstein condensate (BEC), which is described by the mean-field Gross-Pitaevskii equations (GPEs) coupled with dipole-dipole interaction (DDI), under strongly anisotropic external confining potentials. The original three dimensions (3D) problem is then reduced to quasi-2D and quasi-1D models for pancake- and cigar-shaped trapping potentials respectively. To compute the ground state, we propose an efficient and accurate algorithm by incorporating the kernel truncation method (KTM) for the dipolar potential evaluation into the projected gradient flow (PGF) method. The long-range dipolar potential is computed efficiently and accurately by KTM with optimal zero-padding factor, and the resulted PGF-KTM algorithm achieves spectral accuracy in the ground states. We compute the ground states in different space dimensions, and confirm the convergence and rates of dimension reduction from 3D to quasi-2D and from 3D to quasi-1D. Extensive numerical results of ground states for BECs with ferromagnetic/antiferromagnetic interaction and various external potentials in 1D/2D/3D are reported.

1. Introduction

Research in dilute cold atomic quantum gases remains very active, especially after the experimental realizations of Bose-Einstein condensate (BEC) in alkali atomic gases in 1995 [1]. In recent years, BEC with internal degrees of freedom, the so-called spinor BEC, has attracted much attention experimentally and theoretically [13]. Spinor BEC opens up a new paradigm where the order parameter of condensates is described by a multi-component vector [26]. This can be possible by optically trapping cold atoms where all hyperfine states are liberated, while magnetic trapping freezes its freedom. One of the salient features of gaseous BECs is the magnetic dipole-dipole interaction, which is long-range, anisotropic, and exerts a tensor force. There is everlasting enthusiasm in studying the ground state of spinor dipolar BECs theoretically since the observation of a dipolar BEC in a system of spin-polarized ^{52}Cr atoms [19,22,27]. The dipolar interaction is expected to yield rich and novel phenomena when combined with spin degrees of freedom, such as the Einstein-de Haas effect [21], ground-state spin textures and mass currents [22].

A spin-F ($F \in \mathbb{N}$) dipolar condensate is described by a generalized coupled GPE, which consists of $2F + 1$ equations, each governing one of the $2F + 1$ hyperfine states within the mean-field approximation. The mathematical model for spin-1 BEC with magnetic

* Corresponding author.
E-mail addresses: zhixuan_li@stu.scu.edu.cn (Z. Li), qinglin_tang@scu.edu.cn (Q. Tang), wang_hanquan@hotmail.com (H. Wang), Zhang_Yong@tju.edu.cn (Y. Zhang).

https://doi.org/10.1016/j.jcp.2026.114671
Received 6 July 2025; Received in revised form 10 November 2025; Accepted 8 January 2026
Available online 11 January 2026

dipolar-dipolar interaction field is the following nonlocal coupled Gross-Pitaevskii equations [20,32,36]:

$$\mathrm{i}\,\hbar\partial_t\psi_1(\mathbf{x},t) = H_0\psi_1 + (g_sF_z + g_dD_z)\psi_1 + (g_sF_- + g_dD_-)\psi_0, \tag{1.1}$$

$$\mathrm{i}\,\hbar\partial_t\psi_0(\mathbf{x},t) = H_0\psi_0 + (g_sF_+ + g_dD_+)\psi_1 + (g_sF_- + g_dD_-)\psi_{-1}, \tag{1.2}$$

$$\mathrm{i}\,\hbar\partial_t\psi_{-1}(\mathbf{x},t) = H_0\psi_{-1} + (g_sF_+ + g_dD_+)\psi_0 - (g_sF_z + g_dD_z)\psi_{-1}. \tag{1.3}$$

Here $\mathrm{i}=\sqrt{-1}$ is the imaginary unit, $\mathbf{x}=(x,y,z)^\top$ is the Cartesian coordinate vector, t is the time, $\hbar$ is the Planck constant, $\Psi=(\psi_1,\psi_0,\psi_{-1})^\top$ is the time-dependent complex-valued wave function. The Hamiltonian operator $H_0 := -\frac{\hbar^2\nabla^2}{2m} + V(\mathbf{x}) + g_n\rho$ and $\rho = \sum_{j=-1}^{1}|\psi_j|^2$ represents the total density. The trapping potential

$$V(\mathbf{x}) = \frac{1}{2}m(\omega_x^2x^2 + \omega_y^2y^2 + \omega_z^2z^2), \tag{1.4}$$

where ω_x, ω_y and ω_z are the trap frequencies in the $x-$, $y-$, and $z-$direction, respectively. Interaction between atoms of mass m is characterized by the interaction strengths through the "density" channel, $g_n = \frac{4\pi\hbar^2}{m}\cdot\frac{a_0+2a_2}{3}$, and the "spin" channel, $g_s = \frac{4\pi\hbar^2}{m}\cdot\frac{a_2-a_0}{3}$, where a_0 and a_2 are the s-wave scattering length with the total spin 0 (anti-parallel spin collision) and 2 (parallel spin collision) channels, respectively. The mean-field interaction g_n is positive for repulsive interaction and negative for attractive interaction. The spin-exchange interaction g_s is positive for anti-ferromagnetic interaction and negative for ferromagnetic interaction. The dipolar interaction parameter is $g_d = \frac{\mu_0(g_F\mu_B)^2}{3}$ with μ_0, g_F, μ_B being the magnetic permeability of vacuum, the hyperfine g factor and the Bohr magneton, respectively.

Introduce the spin-1 matrices $\mathbf{f}=(f_x,f_y,f_z)^\top$ as

$$f_x = \frac{1}{\sqrt{2}}\begin{pmatrix}0&1&0\\1&0&1\\0&1&0\end{pmatrix},\quad f_y = \frac{\mathrm{i}}{\sqrt{2}}\begin{pmatrix}0&-1&0\\1&0&-1\\0&1&0\end{pmatrix},\quad f_z = \begin{pmatrix}1&0&0\\0&0&0\\0&0&-1\end{pmatrix}, \tag{1.5}$$

and the spin vector $\mathbf{F} := (F_x(\Psi),F_y(\Psi),F_z(\Psi))^\top := (\Psi^{\mathsf{H}}f_x\Psi,\Psi^{\mathsf{H}}f_y\Psi,\Psi^{\mathsf{H}}f_z\Psi)^\top$ (Ψ^{H} is the conjugate transpose of Ψ) of the condensate is given explicitly as

$$F_x = \frac{1}{\sqrt{2}}\left[\bar\psi_1\psi_0 + \bar\psi_0(\psi_1+\psi_{-1}) + \bar\psi_{-1}\psi_0\right],\quad F_y = \frac{\mathrm{i}}{\sqrt{2}}\left[-\bar\psi_1\psi_0 + \bar\psi_0(\psi_1-\psi_{-1}) + \bar\psi_{-1}\psi_0\right],$$

and $F_z = |\psi_1|^2 - |\psi_{-1}|^2$. The effective dipolar field, denoted by $\mathbf{D}=(D_x,D_y,D_z)$, is defined below

$$D_\nu(\mathbf{x}) = \int_{\mathbb{R}^3}\frac{3}{4\pi}\frac{1}{|\mathbf{x}-\mathbf{x}'|^3}\left[F_\nu(\mathbf{x}') - 3\,e_\nu\,\mathbf{F}(\mathbf{x}')\cdot\mathbf{e}\right]\mathrm{d}\mathbf{x}',\ \mathbf{e}=\frac{\mathbf{x}-\mathbf{x}'}{|\mathbf{x}-\mathbf{x}'|},\ \nu=x,y,z. \tag{1.6}$$

Furthermore, we define the transverse magnetization and transverse dipolar field by $F_\pm = (F_x \pm \mathrm{i}F_y)/\sqrt{2}$ and $D_\pm = (D_x \pm \mathrm{i}D_y)/\sqrt{2}$, respectively.

Introduce the following parameters

$$\tilde t = \omega_m t,\quad \tilde{\mathbf{x}} = \mathbf{x}/b_0,\quad b_0 = \sqrt{\hbar/(m\omega_m)},\quad \omega_m = \min\{\omega_x,\omega_y,\omega_z\},$$

and the wave function

$$\tilde\Psi_j(\tilde{\mathbf{x}},\tilde t) = N^{-\frac{1}{2}}b_0^{\frac{3}{2}}\Psi_j(\mathbf{x},t),\quad j=1,0,-1, \tag{1.7}$$

where N is the total number of particles in the condensate. Plugging Eq. (1.7) into equations Eqs. (1.1)–(1.3) and removing all $\sim$, we obtain the dimensionless nonlocal GPEs

$$\mathrm{i}\,\partial_t\Psi(\mathbf{x},t) = \left[-\frac{1}{2}\nabla^2 + V(\mathbf{x}) + \lambda_n\rho + \lambda_s\mathbf{F}\cdot\mathbf{f} + \lambda_d\mathbf{D}\cdot\mathbf{f}\right]\Psi, \tag{1.8}$$

$$\Psi(\mathbf{x},0) = \Psi^{(0)}(\mathbf{x}),\quad \mathbf{x}\in\mathbb{R}^3,$$

where $\mathbf{F}\cdot\mathbf{f} = \sum_\eta F_\eta f_\eta$, $\mathbf{D}\cdot\mathbf{f} = \sum_\nu D_\nu f_\nu$ (we use $\sum_\eta$ and $\sum_\nu$ to denote $\sum_{\eta\in\{x,y,z\}}$ and $\sum_{\nu\in\{x,y,z\}}$ respectively unless otherwise specified). The external trapping potential is

$$V(\mathbf{x}) = \frac{1}{2}(\gamma_x^2x^2 + \gamma_y^2y^2 + \gamma_z^2z^2),$$

with $\gamma_\nu = \frac{\omega_\nu}{\omega_m}$, $\nu=x,y,z$, and the strength of density channel, spin channel and dipole-dipole interaction (DDI) are scaled as $\lambda_n = \frac{4\pi N}{3}\frac{a_0+2a_2}{b_0}$, $\lambda_s = \frac{4\pi N}{3}\frac{a_2-a_0}{b_0}$, $\lambda_d = \frac{\mu_0(g_F\mu_B)^2N}{3\omega_m b_0^3\hbar}$. Using the convolution identity in Appendix A, the effective dipolar field is rewritten as

$$\begin{aligned}D_\nu &= \sum_\eta U_{\eta\nu} * F_\eta = -3\sum_\eta\frac{1}{4\pi|\mathbf{x}|} * (\partial_{\eta\nu}F_\eta) - F_\nu\\ &= -3\sum_\eta\partial_{\eta\nu}\left(\frac{1}{4\pi|\mathbf{x}|} * F_\eta\right) - F_\nu := -3\sum_\eta\partial_{\eta\nu}\varphi_\eta - F_\nu.\end{aligned} \tag{1.9}$$

The DDI convolution kernel $U_{\eta\nu}$ reads as

$$U_{\eta\nu}(\mathbf{x}) = \frac{3}{4\pi}\ \frac{1}{|\mathbf{x}|^3}\left(\delta_{\eta\nu} - 3\frac{x_\eta x_\nu}{|\mathbf{x}|^2}\right), \quad \eta, \nu = x, y, z,$$

where $\delta_{\eta\nu}$ is the Kronecker symbol and φ_η, the Coulomb potential generated by spin density F_η, is defined as follows

$$\varphi_\eta(\mathbf{x}) = \left(\frac{1}{4\pi|\mathbf{x}|} * F_\eta\right)(\mathbf{x}) = \frac{1}{4\pi}\int_{\mathbb{R}^3} \frac{1}{|\mathbf{x}-\mathbf{y}|} F_\eta(\mathbf{y})\mathrm{d}\mathbf{y}. \tag{1.10}$$

It is worth noting that, due to the presence of DDI, the magnetization (or the spin angular momentum) of Eq. (1.8), i.e., $\mathcal{M}(\Psi(\cdot,t)) := \int_{\mathbb{R}^3}\sum_{j=-1}^{1} j|\psi_j(\mathbf{x},t)|^2\,\mathrm{d}\mathbf{x}$ is not conserved [32]. Two important invariants are the *mass*

$$\mathcal{N}(\Psi(\cdot,t)) = \|\Psi(\cdot,t)\|^2 := \sum_{j=-1}^{1}\int_{\mathbb{R}^3} |\psi_j(\mathbf{x},t)|^2\,\mathrm{d}\mathbf{x} \equiv \mathcal{N}(\Psi(\cdot,0)) = 1, \quad t \ge 0, \tag{1.11}$$

and the *energy* per particle

$$\mathcal{E}(\Psi(\cdot,t)) := \int_{\mathbb{R}^3}\left[\sum_{j=-1}^{1}\bar{\psi}_j\left(-\frac{\nabla^2}{2}+V\right)\psi_j + \frac{\lambda_n}{2}\rho^2 + \frac{\lambda_s}{2}|\mathbf{F}|^2\right]\mathrm{d}\mathbf{x} + V_{dd} \equiv \mathcal{E}(\Psi(\cdot,0)), \quad t \ge 0, \tag{1.12}$$

where $|\mathbf{F}|^2 = F_x^2 + F_y^2 + F_z^2$ and the dipolar energy V_{dd} is given explicitly

$$V_{dd} = \frac{\lambda_d}{2}\sum_\eta \int_{\mathbb{R}^3} F_\eta(\mathbf{x})\left[\sum_\nu \int_{\mathbb{R}^3} U_{\eta\nu}(\mathbf{x}-\mathbf{x}')F_\nu(\mathbf{x}')\,\mathrm{d}\mathbf{x}'\right]\mathrm{d}\mathbf{x}.$$

The ground state, denoted as $\Phi^g = (\phi_1^g, \phi_0^g, \phi_{-1}^g)^\top$, is defined as minimizer of the energy functional over constraint manifold $\mathcal{S}$, that is,

$$\Phi^g = \operatorname*{argmin}_{\Phi\in\mathcal{S}} \mathcal{E}(\Phi), \text{ where } \mathcal{S} := \{\Phi = (\phi_1,\phi_0,\phi_{-1})^\top \in (H_0^1(\mathbb{R}^3))^3 \,|\, \|\Phi\|^2 = 1, \mathcal{E}(\Phi) < \infty\}. \tag{1.13}$$

In fact, there exist $\mu = \mu^g$ and $\Phi = \Phi^g$ satisfying the following Euler-Lagrangian equation

$$\mu\Phi = \left[-\frac{1}{2}\nabla^2 + V(\mathbf{x}) + \lambda_n\rho + \lambda_s\mathbf{F}\cdot\mathbf{f} + \lambda_d\mathbf{D}\cdot\mathbf{f}\right]\Phi := \mathbf{H}(\Phi), \tag{1.14}$$

where $\mathbf{H}(\Phi) = (H_1, H_0, H_{-1})^\top$ and the chemical potential μ is computed as $\mu = \sum_{j=-1}^{1}\int_{\mathbb{R}^3}\bar{\phi}_j H_j(\Phi)\mathrm{d}\mathbf{x}$. In addition, Eq. (1.14) is actually a nonlinear eigenvalue problem for (Φ,μ) under the constraint Eq. (1.11), and therefore, the ground state is the eigenfunction with the lowest energy.

Different numerical methods have been developed in the literature to compute the ground state of a single-component BEC. Roughly speaking, they can be divided into the minimization methods based on GP energy and eigenvalue solvers based on Euler-Lagrangian equation. For minimization approach, the ground state is regarded as the solution of a constrained minimization problem, and gradient flow based methods and optimization algorithms are the two main popular approaches. The former includes gradient flow with discrete normalization (GFDN) [5,7], projected gradient flow (PGF) [7], scalar auxiliary variable approach coupled with a penalty term [38], and gradient flow with Lagrange multiplier (GFLM) [23]. The optimization approach includes directly minimizing energy functional [11], Sobolev gradient method [14], Riemannian optimization method [15], preconditioned nonlinear conjugate gradient method [2] and regularized Newton method [35] etc.

Due to presence of the external potential, all spin component F_η are smooth and fast decaying, then the DDI computation boils down to the evaluation of Coulomb potential which is generated by $\partial_{\eta\nu}F_\eta$. During the last decades, various accurate and fast algorithms, starting from the convolution or Fourier integral form, have been proposed, including Nonuniform Fast Fourier transform method [18], Gaussian-Sum based method [16], Kernel Truncation Method (KTM) [33] and anisotropic kernel truncation method [17]. All such algorithms achieve spectral accuracy and share a FFT-like complexity $\mathcal{O}(M\log M)$ with M being the total number of grid points, and have been successfully applied to study various BECs [3,4,9,30,31].

So far as we know, there are few studies on mathematical and numerical study of the ground state for spin-1 dipolar BECs. To compute the ground state numerically, the difficulties lie in the proper treatment of the mass constraint Eq. (1.11) and resolving the hyperfine spatial structure induced by the anisotropic dipole-dipole interaction and spin effects, which correspondingly requires the ground state solver to be accurate enough in space and capable to escape from local minima. The widely-used PGF-based methods treat the mass constraint as a Lagrange multiplier, and have been successfully applied to spinor systems [6,10,12,34]. The PGF-based method allows for flexible spaital-temporal discretizations and proves to be accurate, efficient and robust, therefore, it stands out as a good candidate. As for the computation of dipole-dipole interaction, due to the kernel singularity, convolution non-locality and density anisotropy, accurate and fast evaluation of DDI is quite challenging. Classical PDE-based method encounter "accuracy locking" phenomenon due to the limited accuracy of boundary condition approximation [9]. Thus, we shall turn to integral-based solver, and, among all feasible and efficient algorithms, KTM is the simplest one and has been widely adopted in the physics community [28,29]. This motivates us to extend PGF method by integrating KTM, which can be equipped with optimal zero-padding [24] for better efficiency and stability, for the DDI evaluation, and we can reasonably expect implementation easiness and excellent performance in terms of accuracy and efficiency when computing the ground state.

The paper is organized as follows. In Section 2, one and two dimensional mean-field equations for cigar and pancake-shaped spin-1 dipolar Bose-Einstein condensates are derived via a dimension reduction procedure. In Section 3, we propose an efficient and accurate numerical method for computing the ground state by integrating KTM into PGF. In Section 4, spatial accuracy and convergence rates of the dimension reduction are verified, and detailed ground state results under different potentials from 1D to 3D are reported. Finally, some conclusions are drawn in Section 5.

2. Dimension reduction

In many physical experiments with spin-1 dipolar BECs, the condensates are confined by a strong harmonic trap in one or two axis directions, resulting in a pancake- or cigar-shaped BEC, respectively. Mathematically speaking, this corresponds to the anisotropic potentials $V_\varepsilon(\mathbf{x})$ of the following forms:

Case I (*pancake − shaped*). The potential is strongly confined in the vertical z-direction with

$$V_\varepsilon(\mathbf{x}) = V_{2d}(\mathbf{x}_\perp) + \frac{1}{\varepsilon^2} V_z(\frac{z}{\varepsilon}). \tag{2.1}$$

Case II (*cigar − shaped*). The potential is strongly confined in the horizontal $\mathbf{x}_\perp$-plane with

$$V_\varepsilon(\mathbf{x}) = V_{1d}(z) + \frac{1}{\varepsilon^2} V_\perp(\frac{\mathbf{x}_\perp}{\varepsilon}), \tag{2.2}$$

where $\mathbf{x} = (\mathbf{x}_\perp, z), \mathbf{x}_\perp \in \mathbb{R}^2$ and $0 < \varepsilon \ll 1$ is a small parameter describing the confining strength.

Plugging Eqs. (1.9) into (1.8) and noticing (1.10), we can reformulate nonlocal Eq. (1.8) as the following coupled equations

$$\begin{aligned}
\mathrm{i}\,\partial_t \psi_1(\mathbf{x},t) =& \Big(-\frac{\nabla^2}{2} + V + \lambda_n\rho\Big)\psi_1 + (\lambda_s - \lambda_d)\big(F_z\psi_1 + F_-\psi_0\big) \\
& - 3\lambda_d \sum_\eta \left[\psi_1\big(\partial_{z\eta}\varphi_\eta\big) r g + \frac{1}{\sqrt{2}}\psi_0\big(\partial_{x\eta}\varphi_\eta\big) - \frac{\mathrm{i}}{\sqrt{2}}\psi_0\big(\partial_{y\eta}\varphi_\eta\big)\right], \qquad (2.3)\\
\mathrm{i}\,\partial_t \psi_0(\mathbf{x},t) =& \Big(-\frac{\nabla^2}{2} + V + \lambda_n\rho\Big)\psi_0 + \big(\lambda_s - \lambda_d\big)\big(F_+\psi_1 + F_-\psi_{-1}\big) \\
& - 3\lambda_d \sum_\eta \left[\left(\frac{1}{\sqrt{2}}\psi_1 + \frac{1}{\sqrt{2}}\psi_{-1}\right)\big(\partial_{x\eta}\varphi_\eta\big) + \left(\frac{\mathrm{i}}{\sqrt{2}}\psi_1 - \frac{\mathrm{i}}{\sqrt{2}}\psi_{-1}\right)\big(\partial_{y\eta}\varphi_\eta\big)\right], \qquad (2.4)\\
\mathrm{i}\,\partial_t \psi_{-1}(\mathbf{x},t) =& \Big(-\frac{\nabla^2}{2} + V + \lambda_n\rho\Big)\psi_{-1} + \big(\lambda_s - \lambda_d\big)\big(-F_z\psi_{-1} + F_+\psi_0\big) \\
& - 3\lambda_d \sum_\eta \left[-\psi_{-1}\big(\partial_{z\eta}\varphi_\eta\big) + \frac{1}{\sqrt{2}}\psi_0\big(\partial_{x\eta}\varphi_\eta\big) + \frac{\mathrm{i}}{\sqrt{2}}\psi_0\big(\partial_{y\eta}\varphi_\eta\big)\right], \qquad (2.5)\\
\psi_j(\mathbf{x},0) =& \psi_j^{(0)}(\mathbf{x}), \quad \mathbf{x} \in \mathbb{R}^3, \quad j = 1, 0, -1.
\end{aligned}$$

In such cases, analogous to the dimension-reduction procedure presented in [8], the above Eqs. (2.3)–(2.5) in 3D can be formally reduced to two dimensions (2D) and one dimension (1D), respectively.

2.1. Quasi-2D spin-1 dipolar BEC

In Case I, when $\varepsilon \to 0^+$, evolution of the solution $\Psi(\mathbf{x},t)$ of (2.3)-(2.5) in the z-direction would essentially occur in the ground state mode of $H_z^\varepsilon := -\frac{1}{2}\partial_{zz} + \frac{1}{\varepsilon^2}V_z(\frac{z}{\varepsilon})$, which is spanned by $\omega_{1d}(z) = \varepsilon^{-\frac{1}{2}}\pi^{-\frac{1}{4}}e^{-\frac{z^2}{2\varepsilon^2}}$. We write the factorized wave function as

$$\psi_j(\mathbf{x},t) \approx \psi_j^{2d}(x,y,t)\omega_{1d}(z)e^{-\frac{\mathrm{i}t}{2\varepsilon^2}}, \quad \mathbf{x} \in \mathbb{R}^3, \quad t \geq 0, j = 1, 0, -1. \tag{2.6}$$

Define $\Psi^{2d} = (\psi_1^{2d}, \psi_0^{2d}, \psi_{-1}^{2d})^\top$, $F_\eta^{2d} = (\Psi^{2d})^{\mathsf{H}} F_\eta \Psi^{2d}$, $F_\pm^{2d} = (F_x^{2d} \pm \mathrm{i}\, F_y^{2d})/\sqrt{2}$, $\rho_{2d} = \sum_{j=-1}^1 |\psi_j^{2d}|^2$. Plugging (2.13) into (2.3)–(2.5), here we take (2.3) as an example for brevity. After multiplying both sides by $\omega_{1d}(z)$ and integrating over the z direction, we can obtain a 2D wave equation for ψ_1^{2d}. The integration is straightforward for all but the convolution term because $\int_{\mathbb{R}} \omega_{1d}^2(z)\mathrm{d}z = 1$ and $\int_{\mathbb{R}} \omega_{1d}^4(z)\mathrm{d}z = 1/\sqrt{2\pi}\varepsilon$, in the following we only present the integration of the convolution term

$$\sum_\eta \int_{-\infty}^{\infty} \left[\psi_1^{2d}\omega_{1d}^2\big(\partial_{z\eta}\varphi_\eta\big) + \frac{1}{\sqrt{2}}\psi_0^{2d}\omega_{1d}^2\big(\partial_{x\eta}\varphi_\eta\big) - \frac{\mathrm{i}}{\sqrt{2}}\psi_0^{2d}\omega_{1d}^2\big(\partial_{y\eta}\varphi_\eta\big)\right]\mathrm{d}z. \tag{2.7}$$

Since the Coulomb kernel $\frac{1}{4\pi|\mathbf{x}|}$ happens to be the Green's function of the Laplace operator in 3D, we use the identity $-\nabla^2 U_{3d}(\mathbf{x}) = \delta(\mathbf{x})$. As $U_{3d} * (F_\eta^{2d}\omega_{1d}^2)$ is even in z, $\partial_{z\eta}\Big(U_{3d} * (F_\eta^{2d}\omega_{1d}^2)\Big)$ and $\partial_{\eta z}\Big(U_{3d} * (F_\eta^{2d}\omega_{1d}^2)\Big)$ become odd in z with $\eta = x, y$, thus Eq. (2.7) becomes

$$-\frac{1}{\sqrt{2\pi}\varepsilon}F_z^{2d}\psi_1^{2d} - \int_{-\infty}^{\infty} \psi_1^{2d}\omega_{1d}^2\nabla_\perp^2\big(U_{3d} * (F_z^{2d}\omega_{1d}^2)\big)\mathrm{d}z$$

$$+\sum_{\eta\in\{x,y\}}\int_{-\infty}^{\infty}\psi_0^{2d}\omega_{1d}^2\left[\left(\frac{1}{\sqrt{2}}\partial_{x\eta}-\frac{\mathrm{i}}{\sqrt{2}}\partial_{y\eta}\right)\left(U_{3d}*(F_\eta^{2d}\omega_{1d}^2)\right)\right]\mathrm{d}z, \tag{2.8}$$

where the $\partial_{z\eta}$ and $\partial_{\eta z}$ term disappear because the integral of odd functions vanishes. After expanding the convolution in (2.8) and changing the variables for simplification, we get the mean-field equation for the quasi-2D spin-1 dipolar BEC

$$\begin{aligned}\mathrm{i}\,\partial_t\psi_1^{2d}=&\left(-\frac{\nabla_\perp^2}{2}+V_{2d}+\frac{\lambda_n^{2d}}{\sqrt{2\pi\varepsilon}}\rho_{2d}\right)\psi_1^{2d}+\frac{\left(\lambda_s^{2d}-\lambda_d^{2d}\right)}{\sqrt{2\pi\varepsilon}}F_-^{2d}\psi_0^{2d}+\frac{\left(\lambda_s^{2d}+2\lambda_d^{2d}\right)}{\sqrt{2\pi\varepsilon}}F_z^{2d}\psi_1^{2d}\\&+\frac{3}{2}\lambda_d^{2d}\left[\psi_1^{2d}\nabla_\perp^2\varphi_z^{2d}-\sum_{\eta\in\{x,y\}}\psi_0^{2d}\left(\frac{1}{\sqrt{2}}\partial_{x\eta}-\frac{\mathrm{i}}{\sqrt{2}}\partial_{y\eta}\right)\varphi_\eta^{2d}\right].\end{aligned} \tag{2.9}$$

Similarly, we have

$$\begin{aligned}\mathrm{i}\,\partial_t\psi_0^{2d}=&\left(-\frac{\nabla_\perp^2}{2}+V_{2d}+\frac{\lambda_n^{2d}}{\sqrt{2\pi\varepsilon}}\rho_{2d}\right)\psi_0^{2d}+\left(F_+^{2d}\psi_1^{2d}+F_-^{2d}\psi_{-1}^{2d}\right)\frac{\left(\lambda_s^{2d}-\lambda_d^{2d}\right)}{\sqrt{2\pi\varepsilon}}\\&-\frac{3}{2}\lambda_d^{2d}\sum_{\eta\in\{x,y\}}\left[\psi_1^{2d}\left(\frac{1}{\sqrt{2}}\partial_{x\eta}+\frac{\mathrm{i}}{\sqrt{2}}\partial_{y\eta}\right)\varphi_\eta^{2d}+\psi_{-1}^{2d}\left(\frac{1}{\sqrt{2}}\partial_{x\eta}-\frac{\mathrm{i}}{\sqrt{2}}\partial_{y\eta}\right)\varphi_\eta^{2d}\right],\end{aligned} \tag{2.10}$$

$$\begin{aligned}\mathrm{i}\,\partial_t\psi_{-1}^{2d}=&\left(-\frac{\nabla_\perp^2}{2}+V_{2d}+\frac{\lambda_n^{2d}}{\sqrt{2\pi\varepsilon}}\rho_{2d}\right)\psi_{-1}^{2d}+\frac{\left(\lambda_s^{2d}-\lambda_d^{2d}\right)}{\sqrt{2\pi\varepsilon}}F_+^{2d}\psi_0^{2d}-\frac{\left(\lambda_s^{2d}+2\lambda_d^{2d}\right)}{\sqrt{2\pi\varepsilon}}F_z^{2d}\psi_{-1}^{2d}\\&-\frac{3}{2}\lambda_d^{2d}\left[\psi_{-1}^{2d}\nabla_\perp^2\varphi_z^{2d}+\sum_{\eta\in\{x,y\}}\psi_0^{2d}\left(\frac{1}{\sqrt{2}}\partial_{x\eta}+\frac{\mathrm{i}}{\sqrt{2}}\partial_{y\eta}\right)\varphi_\eta^{2d}\right],\end{aligned} \tag{2.11}$$

where

$$\varphi_\eta^{2d}=U_{2d}*F_\eta^{2d},\quad U_{2d}(x,y)=\frac{2}{(2\pi)^{3/2}}\int_0^\infty\frac{e^{-\frac{s^2}{2}}}{\sqrt{|\mathbf{x}_\perp|^2+\varepsilon^2 s^2}}\mathrm{d}s.$$

The strength of density channel, spin channel and dipole-dipole interaction are scaled as

$$\lambda_n^{2d}=\frac{4\pi N(a_0+2a_2)}{3b_\perp},\quad \lambda_s^{2d}=\frac{4\pi N(a_2-a_0)}{3b_\perp},\quad \lambda_d^{2d}=\frac{\mu_0(g_F\mu_B)^2Nm}{3b_\perp\hbar^2}, \tag{2.12}$$

with $b_\perp=\sqrt{\frac{\hbar}{m\omega_\perp}},\varepsilon=\sqrt{\frac{\omega_\perp}{\omega_z}}$. Since the initial data $\psi_j^{(0)}$ satisfies $\psi_j^{(0)}(\mathbf{x})\approx\psi_j^{2d}(\mathbf{x}_\perp)\omega_{1d}(z)$, multiplying by $\omega_{1d}(z)$ and integrating for z over $\mathbb{R}$, we get the initial data for the Eqs. (2.9)–(2.11) as

$$\psi_j^{2d}(\mathbf{x}_\perp,0)=\int_{\mathbb{R}}\psi_j^{(0)}(\mathbf{x}_\perp,z)\omega_{1d}(z)\,\mathrm{d}z,\quad \mathbf{x}_\perp\in\mathbb{R}^2.$$

Associated to the quasi-2D Eqs. (2.9)–(2.11), the *energy* is

$$\begin{aligned}\mathcal{E}(\Psi^{2d}):=\int_{\mathbb{R}^2}\Bigg\{&\sum_{j=-1}^{1}\bar{\psi}_j^{2d}\left(-\frac{\nabla_\perp^2}{2}+V_{2d}\right)\psi_j^{2d}+\frac{\lambda_n^{2d}}{\sqrt{2\pi\varepsilon}}\rho_{2d}^2+\frac{\lambda_s^{2d}-\lambda_d^{2d}}{\sqrt{2\pi\varepsilon}}\left|\mathbf{F}^{2d}\right|^2+\frac{3\lambda_d^{2d}}{\sqrt{2\pi\varepsilon}}\left|F_z^{2d}\right|^2\\&+\frac{3}{2}\lambda_d^{2d}\left[\nabla_\perp^2\varphi_z^{2d}F_z^{2d}-\sum_{\eta\in\{x,y\}}\left(\partial_{x\eta}\varphi_\eta^{2d}F_x^{2d}+\partial_{y\eta}\varphi_\eta^{2d}F_y^{2d}\right)\right]\Bigg\}\mathrm{d}\mathbf{x}_\perp.\end{aligned}$$

The ground state Φ^g is defined as

$$\Phi^g=\operatorname*{argmin}_{\Phi\in S}\mathcal{E}(\Phi),\ \text{where } S:=\{\Phi=(\phi_1,\phi_0,\phi_{-1})^\top\in(H_0^1(\mathbb{R}^2))^3\,|\,\|\Phi\|^2=1,\mathcal{E}(\Phi)<\infty\}.$$

2.2. Quasi-1D spin-1 dipolar BEC

In Case II, evolution of the solution $\Psi(\mathbf{x}_\perp,z,t)$ of Eqs. (2.3)–(2.5) in the $\mathbf{x}_\perp$-direction would essentially occur in the ground state mode of $H_\perp^\varepsilon:=-\frac{1}{2}\Delta_\perp+\frac{1}{\epsilon^2}V_\perp(\frac{\mathbf{x}_\perp}{\epsilon})$, which is spanned by $\omega_{2d}(\mathbf{x}_\perp)=\varepsilon^{-1}\pi^{-\frac{1}{2}}e^{-\frac{|\mathbf{x}_\perp|^2}{2\epsilon^2}}$. The wave function separates into

$$\psi_j(\mathbf{x},t)\approx\psi_j^{1d}(z,t)\omega_{2d}(\mathbf{x}_\perp)e^{-\frac{\mathrm{i}t}{\epsilon^2}},\quad \mathbf{x}\in\mathbb{R}^3,\quad t\geq0,\quad j=1,0,-1. \tag{2.13}$$

Define $\Psi^{1d}=(\psi_1^{1d},\psi_0^{1d},\psi_{-1}^{1d})^\top$, $F_\eta^{1d}=(\Psi^{1d})^{\mathsf{H}}F_\eta\Psi^{1d}$, $F_\pm^{1d}=(F_x^{1d}\pm\mathrm{i}\,F_y^{1d})/\sqrt{2}$, $\rho_{1d}=\sum_{j=-1}^1|\psi_j^{1d}|^2$. Plugging (2.6) into (2.3)-(2.5), here we take (2.3) as an example for brevity. After multiplying both sides by $\omega_{2d}(\mathbf{x}_\perp)$ and integrating over the $x-y$ plane, we can obtain an equation in z only. The integration is straightforward for all but the convolution term because $\int_{\mathbb{R}^2}\omega_{2d}^2(x,y)\mathrm{d}x\mathrm{d}y=1$ and $\int_{\mathbb{R}^2}\omega_{2d}^4(x,y)\mathrm{d}x\mathrm{d}y=1/2\pi\varepsilon^2$, in the following we only present the integration of the convolution term

$$\sum_\eta\int_{\mathbb{R}^2}\left[\psi_1^{1d}\omega_{2d}^2\left(\partial_{z\eta}\varphi_\eta\right)+\frac{1}{\sqrt{2}}\psi_0^{1d}\omega_{2d}^2\left(\partial_{x\eta}\varphi_\eta\right)-\frac{\mathrm{i}}{\sqrt{2}}\psi_0^{1d}\omega_{2d}^2\left(\partial_{y\eta}\varphi_\eta\right)\right]\mathrm{d}x\mathrm{d}y. \tag{2.14}$$

We recall the symmetry of U_{3d} and ω_{2d} in x and y, and U_{3d} is the Green's function of the Poisson equation. It is worth noting that $F_\eta^{1d}\omega_{2d}^2$ is an even function respect to x and y, and so is $U_{3d} * (F_\eta^{1d}\omega_{2d}^2)$, which implies that the partial derivatives $\partial_{xy}, \partial_{xz}, \partial_{yz}$ of $U_{3d} * (F_\eta^{1d}\omega_{2d}^2)$ are odd functions in x and y. Thus Eq. (2.14) becomes

$$-\frac{1}{4\pi\epsilon^2}\psi_0^{1d}F_-^{1d} + \int_{\mathbb{R}^2}\omega_{2d}^2\Big[\psi_1^{1d}\partial_{zz}\big(U_{3d} * (F_z^{1d}\omega_{2d}^2)\big) - \frac{1}{2}\psi_0^{1d}\partial_{zz}\big(U_{3d} * (F_-^{1d}\omega_{2d}^2)\big)\Big]\mathrm{d}x\mathrm{d}y, \tag{2.15}$$

because the integral of odd functions vanishes. After expanding the convolution in Eq. (2.15) and changing the variables for simplification, we get the mean-field equation for a quasi-1D dipolar BEC

$$\begin{aligned}\mathrm{i}\,\partial_t\psi_1^{1d} =& \left(-\frac{1}{2}\partial_{zz} + V_{1d}(z) + \frac{\lambda_n^{1d}}{2\pi\epsilon^2}\rho_{1d}\right)\psi_1^{1d} + \frac{\left(\lambda_s^{1d}-\lambda_d^{1d}\right)}{2\pi\epsilon^2}F_z^{1d}\psi_1^{1d} + \frac{\left(2\lambda_s^{1d}+\lambda_d^{1d}\right)}{4\pi\epsilon^2}F_-^{1d}\psi_0^{1d}\\ &- \frac{3}{2\pi}\lambda_d^{1d}\left(\psi_1^{1d}\partial_{zz}\varphi_z^{1d} - \frac{1}{2}\psi_0^{1d}\partial_{zz}\varphi_-^{1d}\right).\end{aligned} \tag{2.16}$$

Similarly, we obtain

$$\begin{aligned}\mathrm{i}\,\partial_t\psi_0^{1d} =& \left(-\frac{1}{2}\partial_{zz} + V_{1d}(z) + \frac{\lambda_n^{1d}}{2\pi\epsilon^2}\rho_{1d}\right)\psi_0^{1d} + \frac{\left(2\lambda_s^{1d}+\lambda_d^{1d}\right)}{4\pi\epsilon^2}\left(F_+^{1d}\psi_1^{1d} + F_-^{1d}\psi_{-1}^{1d}\right)\\ &+ \frac{3}{4\pi}\lambda_d^{1d}\left(\psi_1^{1d}\partial_{zz}\varphi_+^{1d} + \psi_{-1}^{1d}\partial_{zz}\varphi_-^{1d}\right),\end{aligned} \tag{2.17}$$

$$\begin{aligned}\mathrm{i}\,\partial_t\psi_{-1}^{1d} =& \left(-\frac{1}{2}\partial_{zz} + V_{1d}(z) + \frac{\lambda_n^{1d}}{2\pi\epsilon^2}\rho_{1d}\right)\psi_{-1}^{1d} - \frac{\left(\lambda_s^{1d}-\lambda_d^{1d}\right)}{2\pi\epsilon^2}F_z^{1d}\psi_{-1}^{1d} + \frac{\left(2\lambda_s^{1d}+\lambda_d^{1d}\right)}{4\pi\epsilon^2}F_+^{1d}\psi_0^{1d}\\ &+ \frac{3}{2\pi}\lambda_d^{1d}\left(\psi_{-1}^{1d}\partial_{zz}\varphi_z^{1d} + \frac{1}{2}\psi_0^{1d}\partial_{zz}\varphi_+^{1d}\right),\end{aligned} \tag{2.18}$$

where

$$\varphi_\nu^{1d} = U_{1d} * F_\nu^{1d}, \quad \varphi_\pm^{1d} = U_{1d} * F_\pm^{1d}, \quad U_{1d}(z) = \frac{1}{4\epsilon^2}\int_0^\infty \frac{e^{-\frac{\mathrm{u}}{2\epsilon^2}}}{\sqrt{z^2+\mathrm{u}}}\mathrm{d}\mathrm{u}.$$

The strength of density channel, spin channel and dipole-dipole interaction are scaled as

$$\lambda_n^{1d} = \frac{4\pi N(a_0+2a_2)}{3b_z}, \quad \lambda_s^{1d} = \frac{4\pi N(a_2-a_0)}{3b_z}, \quad \lambda_d^{1d} = \frac{\mu_0(g_F\mu_B)^2Nm}{3b_z\hbar^2}, \tag{2.19}$$

with $b_z = \sqrt{\frac{\hbar}{m\omega_z}}, \epsilon = \sqrt{\frac{\omega_z}{\omega_\perp}}$. Since the initial data $\psi_j^{(0)}$ satisfies $\psi_j^{(0)}(\mathbf{x}) \approx \psi_j^{1d}(z)\omega_{2d}(\mathbf{x}_\perp)$, multiplying by $\omega_{2d}(\mathbf{x}_\perp)$ and integrating for $\mathbf{x}_\perp$ over $\mathbb{R}^2$, we get the initial data for the (2.9)-(2.11) as

$$\psi_j^{1d}(z,0) = \int_{\mathbb{R}^2}\psi_j^{(0)}(\mathbf{x}_\perp, z)\omega_{2d}(\mathbf{x}_\perp)\,\mathrm{d}\mathbf{x}_\perp, \quad z\in\mathbb{R}.$$

Associated to the quasi-1D (2.9)-(2.11), the *energy* is

$$\begin{aligned}\mathcal{E}(\Psi^{1d}) :=& \int_{\mathbb{R}}\left\{\sum_{j=-1}^{1}\bar{\psi}_j^{1d}\left(-\frac{\partial_{zz}}{2} + V_{1d}\right)\psi_j^{1d} + \frac{\lambda_n^{1d}}{2\pi\epsilon^2}\rho_{1d}^2 + \frac{\lambda_s^{1d}-\lambda_d^{1d}}{2\pi\epsilon^2}\left|\mathbf{F}^{1d}\right|^2 + \frac{3\lambda_d^{1d}}{2\pi\epsilon^2}\left|F_-^{1d}\right|^2\right.\\ &\left.-\frac{3}{2\pi}\lambda_d^{1d}\left[\partial_{zz}\varphi_z^{1d}F_z^{1d} - \frac{1}{2}\sum_{\eta\in\{x,y\}}\partial_{zz}\varphi_\eta^{1d}F_\eta^{1d}\right]\right\}\mathrm{d}z.\end{aligned}$$

The ground state Φ^g is defined as

$$\Phi^g = \operatorname*{argmin}_{\Phi\in S}\mathcal{E}(\Phi), \text{ where } S := \{\Phi = (\phi_1,\phi_0,\phi_{-1})^\top \in (H_0^1(\mathbb{R}))^3 \,|\, \|\Phi\|^2 = 1, \mathcal{E}(\Phi) < \infty\}.$$

3. Numerical algorithm

In this section, we are inspired by the work in [7] to propose the projected gradient flow (PGF) method as an efficient and accurate numerical implementation for computing the ground states of spin-1 dipolar BECs. The basic idea is to evolve the vector wave function by iterating a two-step procedure based on a first-order time splitting of the PGF.

3.1. Projected gradient flow

We first generalize the PGF to the spin-1 dipolar case for $\Phi(\mathbf{x},t) = (\phi_1(\mathbf{x},t),\phi_0(\mathbf{x},t),\phi_{-1}(\mathbf{x},t))^\top$:

$$\partial_t\phi_j(\mathbf{x},t) = -H_j(\Phi) + \mu_\Phi(t)\phi_j, \quad \mathbf{x}\in\mathbb{R}^d, \quad t>0, \quad j=1,0,-1, \tag{3.1}$$

with the initial condition $\Phi(\mathbf{x},0)=\Phi^{(0)}(\mathbf{x})\in S$. Here, $\mu_\Phi(t)$ is chosen such that the above PGF is mass (or normalization) conservative, it can be computed as

$$\mu_\Phi(t)=\frac{P_\Phi(t)}{N_\Phi(t)}, \tag{3.2}$$

with

$$N_\Phi(t)=\sum_{j=-1}^{1}\int_{\mathbb{R}^d}\bar{\phi}_j\phi_j\mathrm{d}\mathbf{x},\quad P_\Phi(t)=\sum_{j=-1}^{1}\int_{\mathbb{R}^d}\bar{\phi}_j H_j(\Phi)\mathrm{d}\mathbf{x}. \tag{3.3}$$

It is easy to show that the PGF Eq. (3.1) is mass-conservative and energy-diminishing:

Proposition 3.1. *For a given initial data $\Phi(\mathbf{x},t=0)=\Phi^{(0)}(\mathbf{x})\in S$, if the solution $\Phi(\cdot,t)$ of the PGF Eq. (3.1) has at least one nonzero components for all $t\geq 0$, then*

$$\mathcal{N}(\Phi(\cdot,t))\equiv 1,\quad \mathcal{E}(\Phi(\cdot,t))\leq\mathcal{E}(\Phi(\cdot,s)),\quad \forall t\geq s\geq 0.$$

Proof. Using Eqs. (3.1)–(3.3), a direct calculation shows that

$$\frac{\mathrm{d}}{\mathrm{d}t}\mathcal{N}(\Phi(\cdot,t))=2\sum_{j=-1}^{1}\mathrm{Re}\int_{\mathbb{R}^d}\overline{\phi}_j\partial_t\phi_j\mathrm{d}\mathbf{x}=2\big(-P_\Phi(t)+N_\Phi(t)\cdot\mu_\Phi(t)\big)=0, \tag{3.4}$$

so that the total mass is conserved. Further, from Eqs. (3.1) and (3.4), we have

$$\begin{aligned}\frac{\mathrm{d}}{\mathrm{d}t}\mathcal{E}(\Phi(\cdot,t))&=2\sum_{j=-1}^{1}\mathrm{Re}\int_{\mathbb{R}^d}\frac{\delta\mathcal{E}(\Phi)}{\delta\phi_j}\partial_t\phi_j\mathrm{d}\mathbf{x}=2\sum_{j=-1}^{1}\mathrm{Re}\int_{\mathbb{R}^d}\overline{H_j(\Phi)}\partial_t\phi_j\mathrm{d}\mathbf{x}\\&=2\sum_{j=-1}^{1}\mathrm{Re}\int_{\mathbb{R}^d}\overline{(H_j(\Phi)-\mu_\Phi(t)\phi_j)}\partial_t\phi_j\mathrm{d}\mathbf{x}\\&=-2\sum_{j=-1}^{1}\int_{\mathbb{R}^d}\overline{(H_j(\Phi)-\mu_\Phi(t)\phi_j)}(H_j(\Phi)-\mu_\Phi(t)\phi_j)\mathrm{d}\mathbf{x}\leq 0,\end{aligned}$$

which implies the energy-diminishing property. □

Similar to the PGF for spin-1 cases [12], it is possible to design a suitable full discretization scheme for Eq. (3.1) in general spin-1 dipolar cases to obtain the mass-conservation and energy-diminishing property in the discretized level. However, in such a scheme, the nonlinear terms must be discretized in very special ways, and thus a fully nonlinear system has to be solved at each time step. This is a little tedious from a computational point of view.

3.2. Semi-discretization in time

Let $t_n=n\tau$ for $n=0,1,2,\ldots$ with $\tau>0$ a given time step length. Denoting $\Phi^n=(\phi_1^n,\phi_0^n,\phi_{-1}^n)^\top(n=1,2,\ldots)$ as the numerical approximation of the solution $\Phi(\cdot,t_n)$ of the PGF Eq. (3.1), we compute Φ^{n+1} from Φ^n via the following two-step procedure:

Step 1: Evolution. Starting at $\Phi(\cdot,t_n)=\Phi^n$, over the time interval $[t_n,t_{n+1}]$, the chemical potential $\mu_{\Phi^n}=\mu_\Phi(t_n)$ is explicitly given in Eq. (3.2). For efficiency and simplicity, we adopt the following backward-forward Euler scheme:

$$\frac{\phi_1^*-\phi_1^n}{\tau}=\frac{1}{2}\nabla^2\phi_1^*-\big(V+\lambda_n\rho^n+\lambda_s F_z^n+\lambda_d D_z^n\big)\phi_1^n-(\lambda_s F_-^n+\lambda_d D_-^n)\phi_0^n+\mu_{\Phi^n}\phi_1^n, \tag{3.5}$$

$$\frac{\phi_0^*-\phi_0^n}{\tau}=\frac{1}{2}\nabla^2\phi_0^*-\big(V+\lambda_n\rho^n\big)\phi_0^n-(\lambda_s F_+^n+\lambda_d D_+^n)\phi_1^n-(\lambda_s F_-^n+\lambda_d D_-^n)\phi_{-1}^n+\mu_{\Phi^n}\phi_0^n, \tag{3.6}$$

$$\frac{\phi_{-1}^*-\phi_{-1}^n}{\tau}=\frac{1}{2}\nabla^2\phi_{-1}^*-\big(V+\lambda_n\rho^n-\lambda_s F_z^n-\lambda_d D_z^n\big)\phi_{-1}^n-(\lambda_s F_+^n+\lambda_d D_+^n)\phi_0^n+\mu_{\Phi^n}\phi_{-1}^n. \tag{3.7}$$

Step 2: Projection. Choose projection constants $\sigma_j^n(j=1,0,-1)$ to define

$$\Phi^{n+1}:=\mathrm{diag}(\sigma_1^n,\sigma_0^n,\sigma_{-1}^n)\Phi^*. \tag{3.8}$$

Here the projection constants $\sigma_j^n(j=-1,0,1)$ are chosen such that the mass constraint Eq. (1.11) is exactly satisfied at Φ^{n+1}, i.e., $\mathcal{N}(\Phi^{n+1})=\|\Phi(\cdot,t_{n+1})\|^2=1$. Combining Eq. (3.8), we obtain

$$\sum_{j=-1}^{1}(\sigma_j^n)^2\|\phi_j^*\|^2=1. \tag{3.9}$$

There are three unknowns and only one equation in the above nonlinear system, so the solution is still undetermined. In order to determine the projection constants σ_j^n uniquely, we need to find additional equations. Analogous to [10], based on the fact that the chemical potentials are the same, we propose to use the following equations as the normalization condition (see details in Appendix B):

$$\sigma_1^n=\sigma_0^n=\sigma_{-1}^n. \tag{3.10}$$

Solving the nonlinear system Eqs. (3.9) and (3.10), we get explicitly the projection constants as

$$\sigma_1^n = \sigma_0^n = \sigma_{-1}^n = \left(\|\phi_1^*\|^2 + \|\phi_0^*\|^2 + \|\phi_{-1}^*\|^2\right)^{-\frac{1}{2}}. \tag{3.11}$$

The practical stopping criterion

$$\frac{\|\Phi^{n+1} - \Phi^n\|}{\tau} \le \varepsilon_{\text{tol}}, \tag{3.12}$$

where the tolerance ε_{tol} is a small parameter. It is clear that Eqs. (3.5)–(3.7) together with the stopping criterion Eq. (3.12) correctly captures the Euler-Lagrange Eq. (1.14).

3.3. Spatial discretization by Fourier spectral method

Due to the external trapping potential, the wave function Φ decays exponentially fast at the far field. Therefore, we can reasonably truncate the whole space $\mathbb{R}^d$ into a bounded rectangular domain Ω and impose periodic boundary conditions on the wave function. Then we can readily apply the Fourier pseudo-spectral method for spatial discretization in this section. We choose $\Omega = [-L, L]^d$ with uniform mesh size $h = 2L/M$, where M is an even number. Define the following sets of indices and grids points

$$\begin{aligned}
\mathcal{Q}_M^d &= \left\{(\ell_1, \ell_2, \dots, \ell_d) \in \mathbb{Z}^d | 0 \le \ell_j \le M-1, j = 1, \dots, d\right\},\\
\mathcal{I}_M^d &= \left\{(k_1, k_2, \dots, k_d) \in \mathbb{Z}^d | -M/2 \le k_j \le M/2-1, j = 1, \dots, d\right\},\\
\mathcal{T}_M^d &= \left\{(x_1, x_2, \dots, x_d) | x_j = -L + \ell_j h, (\ell_1, \ell_2, \dots, \ell_d) \in \mathcal{Q}_M^d\right\}.
\end{aligned}$$

For the sake of simplicity, we take 3D Fourier spectral method as an example and introduce the Fourier basis functions as

$$W_{\mathbf{k}}(\mathbf{x}) := \prod_{v=x,y,z} e^{\mathrm{i}\upsilon_{k_v}^v (v+L)}, \quad \mathbf{k} = (k_x, k_y, k_z) \in \mathcal{I}_M^3,$$

with $\upsilon_{k_v}^v = \pi k_v / L$. The Fourier pseudo-spectral approximation of the wave function $\phi_j (j = 1, 0, -1)$ as well as its derivatives at $\mathbf{x}_{mnl} \in \mathcal{T}_M^3$ are respectively given by

$$\begin{aligned}
\phi_j(\mathbf{x}_{mnl}) \approx \widetilde{\phi_j}(\mathbf{x}_{mnl}) &:= \sum_{\mathbf{k}\in\mathcal{I}_M^3} (\widehat{\phi_j})_{\mathbf{k}} W_{\mathbf{k}}(\mathbf{x}_{mnl}), \quad (m,n,l) \in \mathcal{Q}_M^3,\\
\partial_v \phi_j(\mathbf{x}_{mnl}) \approx [\![\partial_v]\!]\widetilde{\phi_j}(\mathbf{x}_{mnl}) &:= \sum_{\mathbf{k}\in\mathcal{I}_M^3} (\mathrm{i}\,\upsilon_{k_v}^v)(\widehat{\widetilde{\phi_j}})_{\mathbf{k}} W_{\mathbf{k}}(\mathbf{x}_{mnl}),\\
\partial_{\eta v}\phi_j(\mathbf{x}_{mnl}) \approx [\![\partial_{\eta v}]\!]\widetilde{\phi_j}(\mathbf{x}_{mnl}) &:= -\sum_{\mathbf{k}\in\mathcal{I}_M^3} (\upsilon_{k_\eta}^\eta)(\upsilon_{k_v}^v)(\widehat{\widetilde{\phi_j}})_{\mathbf{k}} W_{\mathbf{k}}(\mathbf{x}_{mnl}), \quad \eta, v = x, y, z,
\end{aligned}$$

where the discrete Fourier coefficients $(\widehat{\phi_j})_{\mathbf{k}}$ are given by

$$(\widehat{\phi_j})_{\mathbf{k}} = \frac{1}{M^3} \sum_{(m,n,l)\in\mathcal{Q}_M^3} \phi_j(\mathbf{x}_{mnl}) \overline{W}_{\mathbf{k}}(\mathbf{x}_{mnl}).$$

Meanwhile, we also need operators $[\![\nabla]\!] := ([\![\partial_x]\!], [\![\partial_y]\!], [\![\partial_z]\!])^\top$ and $[\![\Delta]\!] := [\![\partial_x^2]\!] + [\![\partial_y^2]\!] + [\![\partial_z^2]\!]$, which are applied to the approximation $\widetilde{\phi_j}$ of ϕ_j:

$$\nabla\phi_j(\mathbf{x}_{mnl}) \approx [\![\nabla]\!]\widetilde{\phi_j}(\mathbf{x}_{mnl}), \quad \Delta\phi_j(\mathbf{x}_{mnl}) \approx [\![\Delta]\!]\widetilde{\phi_j}(\mathbf{x}_{mnl}), \quad (m,n,l) \in \mathcal{Q}_M^3.$$

To simplify the presentation, we drop the notation "[[]]" in the above-mentioned operators.

3.4. Fast computation of the effective dipolar field

The kernel truncation method (KTM) is a commonly-used algorithm to compute the convolution-type nonlocal potential [3]. Since the wave function decays exponentially fast at the far field, we assume that the spin component $F_\eta (\eta = x, y, z)$ is compactly supported in $\mathbf{R}_L := [-L, L]^d$. For simplicity of implementation, we compute the ground states Φ and the DDI φ_η on the same domain and uniform mesh grid. The nonlocal potential can be computed as

$$\begin{aligned}
\varphi_\eta(\mathbf{x}) &= \int_{\mathbb{R}^d} U(\mathbf{x}-\mathbf{y}) F_\eta(\mathbf{y})\mathrm{d}\mathbf{y} = \int_{\mathbf{R}_L} U(\mathbf{x}-\mathbf{y}) F_\eta(\mathbf{y})\mathrm{d}\mathbf{y}\\
&= \int_{\mathbf{x}+\mathbf{R}_L} U(\mathbf{y}) F_\eta(\mathbf{x}-\mathbf{y})\mathrm{d}\mathbf{y} = \int_{\mathcal{B}_G} U(\mathbf{y}) F_\eta(\mathbf{x}-\mathbf{y})\mathrm{d}\mathbf{y}, \quad \mathbf{x} \in \mathbf{R}_L,
\end{aligned} \tag{3.13}$$

where $\mathcal{B}_G$ is a ball centered at the origin with radius $G := \max_{\mathbf{x},\mathbf{y}\in\mathbf{R}_L} |\mathbf{x}-\mathbf{y}| = 2\sqrt{d}L$ being the diameter of $\mathbf{R}_L$. To compute Eq. (3.13), one needs to approximate the spin component $F_\eta(\mathbf{x})$ on domain $\mathbf{R}_{\text{ess}} := \mathbf{R}_{(2\sqrt{d}+1)L}$ because $\mathbf{x}-\mathbf{y} \in \mathbf{R}_{(2\sqrt{d}+1)L}$ for any $\mathbf{x} \in \mathbf{R}_L$ and $\mathbf{y} \in \mathcal{B}_G$. It is natural to extend the function $F_\eta(\mathbf{x})$ to $\mathbf{R}_{\text{ess}}$ by zero-padding and apply the Fourier spectral method therein. In fact,

by utilizing periodicity of Fourier series [24], we only need to zero-pad to domain $\mathbf{R}_{SL}$ with $S = \lceil \sqrt{d}+1 \rceil$ (rounding up of $\sqrt{d}+1$ to nearest integer), which significantly alleviates the memory/computational costs compared to the original fourfold zero-padding version [33].

On domain $\mathbf{R}_{SL}$, the spin component $F_\eta(\mathbf{x})$ is well resolved by the following finite Fourier series

$$F_\eta(\mathbf{x}) \approx (F_\eta)_M(\mathbf{x}) := \sum_{\mathbf{k}\in I_{SM}^d} \widehat{F_\eta}(\mathbf{k}) e^{\mathrm{i}\frac{\pi\mathbf{k}}{SL}\cdot\mathbf{x}}, \quad \mathbf{x}\in\mathbf{R}_{SL},$$

and the Fourier coefficients are well approximated as follows

$$\widehat{F_\eta}(\mathbf{k}) = \frac{1}{(SM)^d} \sum_{\mathbf{x_p}\in T_{SM}^d} F_\eta(\mathbf{x_p}) e^{-\mathrm{i}\frac{\pi\mathbf{k}}{SL}\cdot\mathbf{x_p}}, \quad \mathbf{k}\in I_{SM}^d.$$

Substituting the Fourier series approximation $(F_\eta)_M$ for F_η in Eq. (3.13), we obtain

$$\begin{aligned}\varphi_\eta(\mathbf{x}) &\approx \int_{B_G} U(\mathbf{y})(F_\eta)_M(\mathbf{x}-\mathbf{y})\mathrm{d}\mathbf{y} = \sum_{\mathbf{k}\in I_{SM}^d}\left(\int_{B_G} U(\mathbf{y}) e^{-\mathrm{i}\frac{\pi\mathbf{k}}{SL}\cdot\mathbf{y}}\mathrm{d}\mathbf{y}\right)\widehat{F_\eta}\, e^{\mathrm{i}\frac{\pi\mathbf{k}}{SL}\cdot\mathbf{x}} \\ &:= \sum_{\mathbf{k}\in I_{SM}^d} \widehat{U_G}(\mathbf{k})\widehat{F_\eta}\, e^{\mathrm{i}\frac{\pi\mathbf{k}}{SL}\cdot\mathbf{x}}, \qquad \mathbf{x}\in\mathbf{R}_L,\end{aligned} \tag{3.14}$$

where $\widehat{U_G}(\mathbf{k})$, Fourier transform of the truncated kernel, is defined as

$$\widehat{U_G}(\mathbf{k}) := \int_{B_G} U(\mathbf{y}) e^{-\mathrm{i}\frac{\pi\mathbf{k}}{SL}\cdot\mathbf{y}}\mathrm{d}\mathbf{y}.$$

When the density manifests strong anisotropic property, that is, the wave function is compactly supported in an anisotropic rectangle $\mathbf{R}_L^{\vec{\gamma}} := \Pi_{j=1}^d [-L\gamma_j, L\gamma_j]^d$ with $\vec{\gamma} = (\gamma_1, \ldots, \gamma_d) \in \mathbb{R}^d$ being the anisotropic vector, the practical optimal zero-padding factor along the jth direction reads as

$$S_j = \left\lceil 1 + \gamma_j^{-1}\sqrt{1+\gamma_2^2+\ldots+\gamma_d^2}\right\rceil. \tag{3.15}$$

As pointed out in [24,33,37], the above algorithm can be written as a discrete convolution of an effective d-dimensional tensor and spin component grid values. Taking the 3D case as an example, we derive the following discrete convolution reformulation

$$\varphi_\eta(x_m, y_n, z_l) = \sum_{(m',n',l')\in I_M^3} T_{m-m',n-n',l-l'}(F_\eta)_{m',n',l'},$$

where the convolution tensor $T_{m,n,l}$ is given explicitly as

$$T_{m,n,l} = \frac{1}{(SM)^3} \sum_{(k_x,k_y,k_z)\in I_{SM}^3} \widehat{U_G}\big(k_x,k_y,k_z\big) e^{\frac{2\pi\mathrm{i}}{SM}(k_x m + k_y n + k_z l)}, \quad (m,n,l)\in I_{2M}^3,$$

and it can be computed by applying the inverse discrete Fourier transform of vector $\{\widehat{U_G}(\mathbf{k}), \mathbf{k}\in I_{SM}^3\} \subset \mathbb{C}^{(SM)^3}$. For the anisotropic case, a very similar convolution structure can be derived following the same procedure. The tensor generation depends on the total zero-padding factor $S_t = S_1S_2S_3$ and it requires $\mathcal{O}(S_t M^3 \log(S_t M^3))$ float operations

It is worthwhile to point out that KTM applies readily once the Fourier transform of the truncated kernel is available analytically or numerically. For example, the effective 1D/2D convolution kernel that is derived from dimension reduction reads as follows

$$U_{1d}(z) = \frac{\sqrt{\pi}}{2\sqrt{2}\varepsilon} e^{\frac{z^2}{2\varepsilon^2}} \mathrm{erfc}\Big(\frac{|z|}{\sqrt{2}\varepsilon}\Big), \quad U_{2d}(r) = \frac{1}{\varepsilon(2\pi)^{3/2}} e^{\frac{r^2}{4\varepsilon^2}} K_0\Big(\frac{r^2}{4\varepsilon^2}\Big), \quad r = |\mathbf{x}_\perp|,$$

where $\mathrm{erfc}(x) = \frac{2}{\sqrt{\pi}}\int_x^\infty e^{-t^2}\mathrm{d}t$ is the complementary error function and $K_0(x)$ is the modified Bessel function of the second-kind.

The Fourier transform of truncated kernel

$$\widehat{(U_{1d})_G}(k) = 2\int_0^G U_{1d}(z)\cos(kz)\,\mathrm{d}z, \quad \widehat{(U_{2d})_G}(k) = 2\pi\int_0^G U_{2d}(r)J_0(kr)r\,\mathrm{d}r, \quad k\in\mathbb{R},$$

where J_0 is Bessel function of the first-kind with index 0, can be evaluated via adaptive Gauss-Kronrod quadrature. The above method is readily applied to nonlocal potential generated by such kernel accurately (up to machine precision) with optimal efficiency achieved with FFT.

4. Numerical results

In this section, we apply the PGF-KTM method Eqs. (3.5)–(3.8) to compute the ground states of spin-1 dipolar BECs from 1D to 3D with different potentials. Two different kinds of interactions, i.e., anti-ferromagnetic and ferromagnetic interactions, are considered. We fix the total number of atoms in the condensate $N = 10^4$ and list the mass m and the s-wave scattering length with the total spin 0 and 2 channels, i.e., a_0, a_2 as follows [19,32,36]:

- **Case I** (Anti-ferromagnetic): ^{23}Na with $m = 3.816 \times 10^{-26}$[kg], $a_0 = 2.646$[nm], $a_2 = 2.911$[nm].
- **Case II** (Ferromagnetic): ^{87}Rb with $m = 1.443 \times 10^{-25}$[kg], $a_0 = 5.387$[nm], $a_2 = 5.313$[nm].

To compute the ground state, there are six commonly-used initial guesses for each component listed as follows

$$(a)\ \phi_a(\mathbf{x}) = \frac{1}{\pi^{d/4}} e^{-\frac{|\mathbf{x}|^2}{2}}, \qquad (b)\ \phi_b(\mathbf{x}) = (x + \mathrm{i}\, y)\phi_a(\mathbf{x}), \quad (\bar{b})\ \phi_{\bar{b}}(\mathbf{x}) = \bar{\phi}_b(\mathbf{x}),$$

$$(c)\ \phi_c(\mathbf{x}) = \frac{\phi_a(\mathbf{x}) + \phi_b(\mathbf{x})}{\|\phi_a(\mathbf{x}) + \phi_b(\mathbf{x})\|}, \quad (\bar{c})\ \phi_{\bar{c}}(\mathbf{x}) = \bar{\phi}_c(\mathbf{x}), \qquad (d)\ \phi_d(\mathbf{x}) = \frac{\phi_g^{\mathrm{TF}}(\mathbf{x})}{\|\phi_g^{\mathrm{TF}}(\mathbf{x})\|},$$

where

$$\phi_g^{\mathrm{TF}}(\mathbf{x}) = \begin{cases} \sqrt{(\mu_g^{\mathrm{TF}} - V(\mathbf{x}))/\lambda_n}, & V(\mathbf{x}) < \mu_g^{\mathrm{TF}}, \\ 0, & \text{otherwise}, \end{cases} \quad \text{with} \quad \mu_g^{\mathrm{TF}} = \frac{1}{2} \begin{cases} (3\lambda_n\gamma_x)^{2/3}, & d = 1, \\ (4\lambda_n\gamma_x\gamma_y)^{1/2}, & d = 2, \\ (15\lambda_n\gamma_x\gamma_y\gamma_z/4\pi)^{2/5}, & d = 3. \end{cases}$$

In computational practice, the initial datum are chosen as $\Phi^0 = (\phi_1^0, \phi_0^0, \phi_{-1}^0)^{\top}/\sqrt{3}$ where ϕ_1^0, ϕ_0^0 and ϕ_{-1}^0 are chosen independently from the above six types. The numerical ground state is selected as the one with the lowest energy. In all computations, the time step is taken as $\tau = 0.1$, the ground state is reached when the stopping criterion Eq. (3.12) is satisfied with $\varepsilon_{\mathrm{tol}} = 10^{-12}$ by default and the mesh size is taken as $h_x = h_y = h_z = 1/16$ uniformly unless otherwise specified.

4.1. Accuracy confirmation

Here, we investigate the spatial accuracy of our numerical method for the 3D, 2D and 1D cases. Let $\Phi_g = (\phi_1^g, \phi_0^g, \phi_{-1}^g)^{\top}$ be the numerical "exact" solution obtained with a very fine mesh $h = 1/16$, and Φ_g^h be the numerical solution obtained with mesh size h. Denote the energy and chemical potential as $E_g := \mathcal{E}(\Phi_g)$ and $\mu_g := \mu(\Phi_g)$ respectively. We use the following relative l^2 norm to measure the error of the ground state:

$$e_h := \left\|\Phi_g - \Phi_g^h\right\|_{l^2} / \left\|\Phi_g\right\|_{l^2}.$$

Example 1 (3D Case). We investigate the spatial accuracy when computing the 3D ground states with the corresponding physical trapping frequencies $\omega_x = \omega_y = \omega_z = 2\pi \times 200$[Hz] and harmonic potential $V(\mathbf{x}) = \frac{1}{2}(x^2 + y^2 + z^2)$ for both anti-ferromagnetic and ferromagnetic cases, and the detailed parameters are listed below:

- **Case I** (Anti-ferromagnetic): ^{23}Na with parameters $\lambda_n = 239.2, \lambda_s = 7.485, \lambda_d = 20.84$.
- **Case II** (Ferromagnetic): ^{87}Rb with parameters $\lambda_n = 879.6, \lambda_s = -4.065, \lambda_d = 15.32$.

The computational domain is chosen as $\Omega = [-8, 8]^3$. Table 1 lists the numerical errors of the ground states for **Case I** and **Case II**. The energy and chemical potential are computed as $E_g = 3.7810$, $\mu_g = 5.0528$ in **Case I**; $E_g = 6.0035$, $\mu_g = 8.2367$ in **Case II**.

From Table 1, we can observe that our scheme is spectrally accurate for computing the ground state of a spin-1 dipolar condensate in 3D.

Example 2 (2D Case). We investigate the spatial accuracy when computing the 2D ground states with the corresponding physical trapping frequencies $\omega_z = 2\pi \times 400$[Hz], $\omega_x = \omega_y = 2\pi \times 20$[Hz], $\varepsilon = \frac{1}{\sqrt{20}}$ and harmonic potential $V(\mathbf{x}) = \frac{1}{2}(x^2 + y^2)$ for both anti-ferromagnetic and ferromagnetic cases, and the detailed parameters Eq. (2.12) are listed below:

- **Case I** (Anti-ferromagnetic): ^{23}Na with parameters $\lambda_n = 75.64, \lambda_s = 2.367, \lambda_d = 6.59$.
- **Case II** (Ferromagnetic): ^{87}Rb with parameters $\lambda_n = 278.1, \lambda_s = -1.285, \lambda_d = 4.846$.

The computational domain is chosen as $\Omega = [-16, 16]^2$. Table 2 lists the numerical errors of the ground states for **Case I** and **Case II**. The energy and chemical potential are computed as $E_g = 4.5350$, $\mu_g = 6.6591$ in **Case I**; $E_g = 8.4545$, $\mu_g = 12.5916$ in **Case II**.

From Table 2, we can observe that our scheme is spectrally accurate for computing the ground state of a spin-1 dipolar condensate in 2D.

Table 1
Numerical errors of the ground states for **Case I** (upper) and **Case II** (lower) in Example 1.

	h	2	1	1/2	1/4	1/8
Case I	e_h	8.5644E-02	6.3392E-03	8.5396E-05	3.7590E-09	7.8352E-13
	$\lvert E_g - E(\Phi_g^h)\rvert$	2.7659E-03	8.6502E-05	6.8430E-08	9.6539E-13	2.0679E-15
	$\lvert \mu_g - \mu(\Phi_g^h)\rvert$	6.2835E-03	4.9762E-05	6.3772E-07	7.5296E-12	1.9822E-15
Case II	e_h	9.2201E-02	6.9257E-03	7.4391E-05	2.4690E-08	3.8746E-13
	$\lvert E_g - E(\Phi_g^h)\rvert$	5.9260E-03	3.9021E-06	8.9972E-09	7.1027E-12	9.2129E-16
	$\lvert \mu_g - \mu(\Phi_g^h)\rvert$	9.6259E-03	4.8910E-05	3.2785E-08	6.2590E-12	2.8749E-15

Table 2
Numerical errors of the ground states for **Case I** (upper) and **Case II** (lower) in Example 2.

	h	2	1	1/2	1/4	1/8
Case I	e_h	3.8357E-02	2.5048E-03	1.5180E-05	5.4849E-10	9.2324E-14
	$\lvert E_g - E(\Phi_g^h)\rvert$	1.5239E-03	7.8268E-05	5.8376E-08	2.6208E-12	1.8255E-15
	$\lvert \mu_g - \mu(\Phi_g^h)\rvert$	2.4872E-03	8.8263E-05	7.6729E-08	5.5294E-12	3.6254E-15
Case II	e_h	9.7937E-02	1.6820E-03	2.9247E-05	2.5051E-09	2.3508E-14
	$\lvert E_g - E(\Phi_g^h)\rvert$	7.3638E-03	4.7629E-05	8.6209E-08	6.2096E-13	2.2054E-15
	$\lvert \mu_g - \mu(\Phi_g^h)\rvert$	2.6753E-03	3.6764E-05	8.8759E-09	7.6729E-13	1.6283E-15

Table 3
Numerical errors of the ground states for **Case I** (upper) and **Case II** (lower) in Example 3.

	h	2	1	1/2	1/4	1/8
Case I	e_h	2.8220E-01	8.8722E-03	1.7702E-05	2.6490E-10	6.2864E-14
	$\lvert E_g - E(\Phi_g^h)\rvert$	4.2706E-03	9.3206E-05	6.9822E-07	3.4479E-12	1.0209E-15
	$\lvert \mu_g - \mu(\Phi_g^h)\rvert$	2.0688E-03	1.7020E-04	2.0024E-07	8.9012E-13	3.8209E-15
Case II	e_h	9.9287E-02	4.7821E-03	7.0982E-05	1.6760E-09	5.8202E-14
	$\lvert E_g - E(\Phi_g^h)\rvert$	2.9931E-03	9.0226E-06	8.0124E-08	6.0281E-13	4.9011E-15
	$\lvert \mu_g - \mu(\Phi_g^h)\rvert$	1.0926E-02	1.7201E-05	2.0271E-07	7.4331E-13	9.8217E-16

Example 3 (1D Case). We investigate the spatial accuracy when computing the 1D ground states with the corresponding physical trapping frequencies $\omega_x = \omega_y = 2\pi \times 400[\text{Hz}], \omega_z = 2\pi \times 8[\text{Hz}]$, $\varepsilon = \frac{1}{\sqrt{50}}$ and harmonic potential $V(x) = x^2/2$ for both anti-ferromagnetic and ferromagnetic cases, and the detailed parameters (2.12) are listed below:

- **Case I** (Anti-ferromagnetic): ^{23}Na with parameters $\lambda_n = 47.839, \lambda_s = 1.497, \lambda_d = 4.168$.
- **Case II** (Ferromagnetic): ^{87}Rb with parameters $\lambda_n = 175.886, \lambda_s = -8.127, \lambda_d = 3.065$.

The computational domain is chosen as $\Omega = [-16, 16]$. Table 3 lists the numerical errors of the ground states for **Case I** and **Case II**. The energy and chemical potential are computed as $E_g = 20.6681$, $\mu_g = 34.4236$ in **Case I**; $E_g = 47.9598$, $\mu_g = 79.9218$ in **Case II**.

From Table 3, we can observe that our scheme is spectrally accurate for computing the ground state of a spin-1 dipolar condensate in 1D.

4.2. Dimension reduction verification

We apply the efficient and accurate numerical method presented in the previous section to confirm numerically convergence and identify convergence rates of the dimension reduction in Section 2. Also, we investigate for both two cases, i.e., anti-ferromagnetic (**Case I**) and ferromagnetic (**Case II**), whose details are the same as Example 1. The presence of strongly anisotropic confining potential will produce anisotropic ground state, and we present isosurface plots of the density function for different ε_ν which describes the confining strength in the ν-direction ($\nu = x, y, z$) respectively in Fig. 1.

Firstly, we consider the dimension reduction from 3D to quasi-2D nonlocal GPEs in terms of ground state. In order to do so, we take the external potential for the 3D nonlocal GPEs (2.3)-(2.5) as

$$V_z(z) = \frac{z^2}{2}, \quad V_{2d}(x, y) = \frac{1}{2}(x^2 + y^2), \quad V_\varepsilon(x, y, z) = \frac{1}{2}(x^2 + y^2 + \frac{z^2}{\varepsilon^4}). \tag{4.1}$$

Denote $\Phi_g := \Phi_g(x, y, z)$ as the ground state of the 3D GPEs (2.3)-(2.5), which are computed $\mathbf{R}_\varepsilon = [-12, 12]^2 \times [-12\varepsilon, 12\varepsilon]$ with mesh sizes $h_x = h_y = 1/16, h_z = \varepsilon/16$. Let $\Phi_g^{2d} := \Phi_g^{2d}(x, y)$ be the ground state of quasi-2D nonlocal GPEs, which are computed on $\Omega = [-12, 12]^2$ with $h_x = h_y = 1/16$. Define $\chi(z) = [\int_{\mathbb{R}^2} |\Phi_g(x, y, z)|^2 \mathrm{d}x\mathrm{d}y]^{1/2}$ as the projections of Φ_g over z-axis.

Table 4 lists errors of $\|\Phi_g - \Phi_g^{2d}\omega_{1d}(z)\|_{l^2}$ and $\|\chi - \omega_{1d}\|_{l^2}$, which demonstrates convergence rates from 3D to quasi-2D nonlocal GPEs in terms of ground states for different ε. From Table 4, we can draw the following conclusions: when the harmonic potential is strongly confined in z-direction, the 3D GPEs converges ***cubically*** to the quasi-2D GPEs in terms of ε, which is exactly the same as that in [25] when $\varepsilon \to 0$. Based on these observations, if one wants to consider the dynamics of electrons trapped in the plane through confinement, quasi-2D nonlocal GPEs is an good approximate 2D model.

Then, we apply our method to numerically identify convergence rates of the dimension reduction from 3D to quasi-1D nonlocal GPEs in terms of ground state. In order to do so, we take the external potential for the 3D nonlocal GPEs (2.3)-(2.5) as

$$V_z(z) = \frac{z^2}{2}, \quad V_{2d}(x, y) = \frac{1}{2}(x^2 + y^2), \quad V_\varepsilon(x, y, z) = \frac{1}{2}(z^2 + \frac{x^2 + y^2}{\varepsilon^4}). \tag{4.2}$$

The ground state of the 3D GPEs (2.3)-(2.5) are computed numerically on a computational domain $\mathbf{R}_\varepsilon = [-12\varepsilon, 12\varepsilon]^2 \times [-12, 12]$ with mesh sizes $h_x = h_y = \varepsilon/16, h_z = 1/16$. Let $\Phi_g^{1d} := \Phi_g^{1d}(z)$ be the ground state of the quasi-1D GPEs, which are computed numerically on $\Omega = [-12, 12]$ with mesh size $h_z = 1/16$.

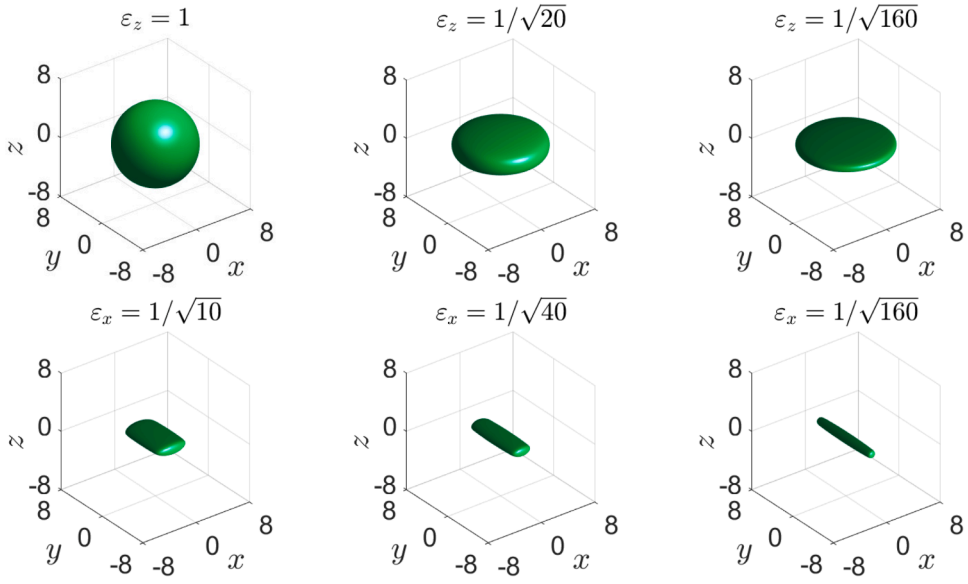

Fig. 1. Isosurface plots of $|\Phi_g(\mathbf{x})|^2 = 0.001$ for different ε_v in **Case II** with fixed $\varepsilon_x = \varepsilon_y = 1$ (top row) and $\varepsilon_z = 1/\sqrt{160}$, $\varepsilon_y = 1$ (bottom row).

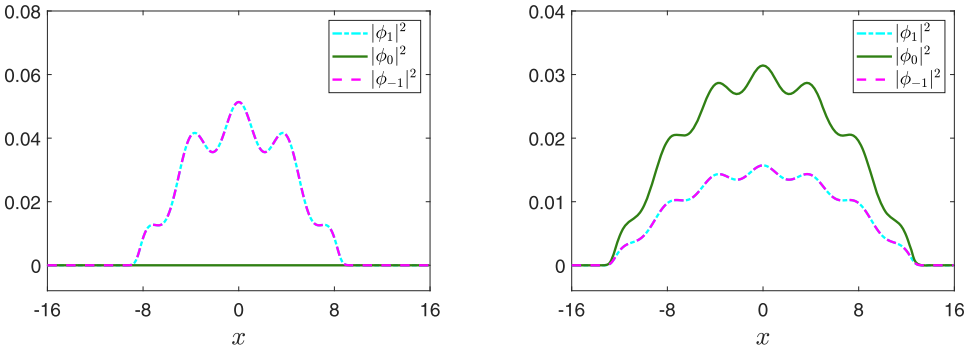

Fig. 2. The densities of ground states in **Case I** (left) and **Case II** (right) for Example 4.

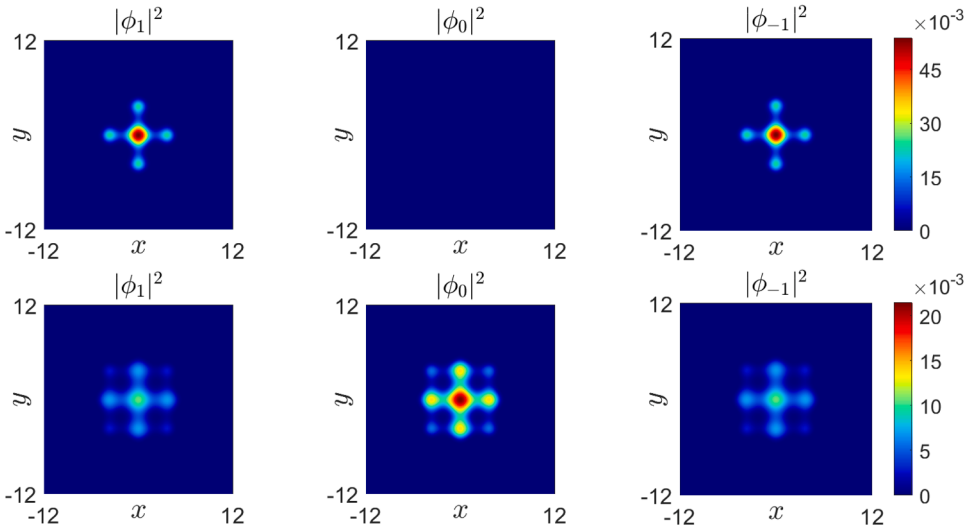

Fig. 3. Contour plots of densities in **Case I** (top row) and **Case II** (bottom row) for optical lattice potential in Example 5.

Table 4
Convergence from 3D to quasi-2D GPEs in terms of ground states: $\|\Phi_g - \Phi_g^{2d}\omega_{1d}(z)\|_{l^2}$ (upper) and $\|\chi - \omega_{1d}\|_{l^2}$ (lower).

ϵ	$\frac{1}{\sqrt{5}}$	$\frac{1}{\sqrt{10}}$	$\frac{1}{\sqrt{20}}$	$\frac{1}{\sqrt{40}}$	$\frac{1}{\sqrt{80}}$	$\frac{1}{\sqrt{160}}$
			$\|\Phi_g - \Phi_g^{2d}\omega_{1d}(z)\|_{l^2}$			
Case I	1.141E-01	4.556E-02	1.781E-02	6.733E-03	2.527E-03	9.124E-04
rate	–	2.65	2.71	2.81	2.83	2.94
Case II	1.532E-01	6.682E-02	2.771E-02	1.083E-02	4.207E-03	1.531E-03
rate	–	2.39	2.54	2.71	2.73	2.92
			$\|\chi - \omega_{1d}\|_{l^2}$			
Case I	9.021E-02	3.546E-02	1.352E-02	4.993E-03	1.817E-03	6.479E-04
rate	–	2.69	2.78	2.87	2.92	2.98
Case II	1.211E-01	4.960E-02	1.981E-02	7.733E-03	2.906E-03	1.054E-03
rate	–	2.58	2.65	2.71	2.82	2.93

Table 5 lists errors of $\|\Phi_g - \Phi_g^{1d}\omega_{2d}(\mathbf{x}_\perp)\|_{l^2}$, which demonstrates convergence rates from 3D to quasi-1D nonlocal GPEs in terms of ground states for different ϵ. From Table 5, we can draw the following conclusions: when the harmonic potential is strongly confined

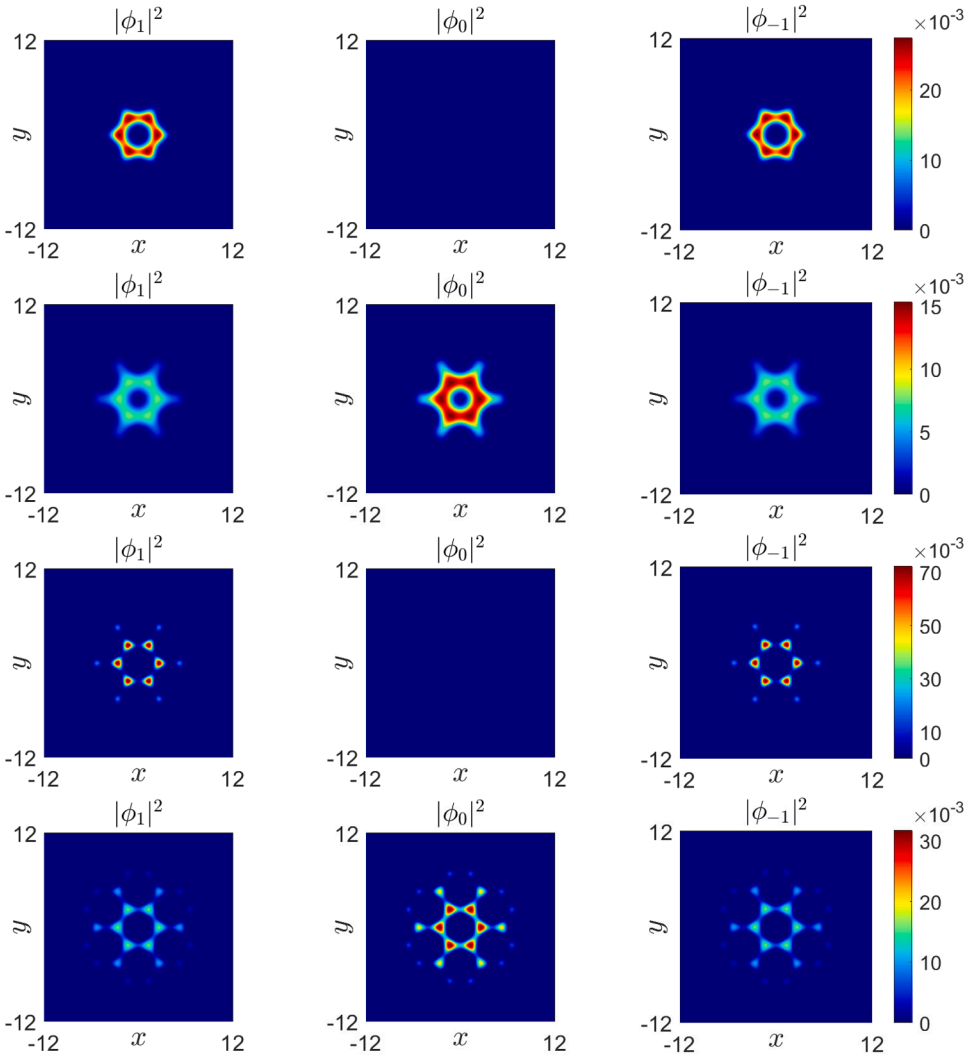

Fig. 4. Contour plots of densities for harmonic + honeycomb potential in Example 5 with $\beta_0 = 5$ in **Case I** (1st row), **Case II** (2nd row) and $\beta_0 = 40$ in **Case I** (3rd row), **Case II** (4th row).

Table 5
Convergence from 3D to quasi-1D GPEs in terms of ground states: $\|\Phi_g - \Phi_g^{1d}\omega_{2d}(z)\|_{l^2}$.

ε	$\frac{1}{\sqrt{5}}$	$\frac{1}{\sqrt{10}}$	$\frac{1}{\sqrt{20}}$	$\frac{1}{\sqrt{40}}$	$\frac{1}{\sqrt{80}}$	$\frac{1}{\sqrt{160}}$
Case I	5.034E-03	2.760E-03	1.448E-03	7.385E-04	3.763E-04	1.891E-04
rate	–	1.73	1.86	1.94	1.95	1.99
Case II	7.209E-03	3.923E-03	2.077E-03	1.086E-03	5.561E-04	2.795E-04
rate	–	1.76	1.83	1.87	1.93	1.98

in the (x, y)-plane, the 3D model converges to quasi-1D GPEs ***quadratically*** in terms of ε on ground states. Based on these observations, if one investigates the dynamics of electrons trapped in the z-axis, the quasi-1D GPEs is an good approximation model.

4.3. Ground states in different dimensions

Here, we study the ground states with ferromagnetic/antiferromagnetic interaction and various external potentials in 1D/2D/3D. By default, the potential function $V(\mathbf{x})$ is chosen as an optical lattice potential

$$V(\mathbf{x}) = \begin{cases} \frac{x^2}{2} + \kappa \sin^2(\frac{\pi x}{4}), & d = 1, \\ \frac{1}{2}(x^2 + y^2) + \kappa\,[\sin^2(\frac{\pi x}{4}) + \sin^2(\frac{\pi y}{4})], & d = 2, \\ \frac{1}{2}(x^2 + y^2 + z^2) + \kappa[\sin^2(\frac{\pi x}{4}) + \sin^2(\frac{\pi y}{4}) + \sin^2(\frac{\pi z}{4})], & d = 3, \end{cases} \tag{4.3}$$

where κ is the depth of the optical lattice, which is fixed as $\kappa = 10$ in our experiments.

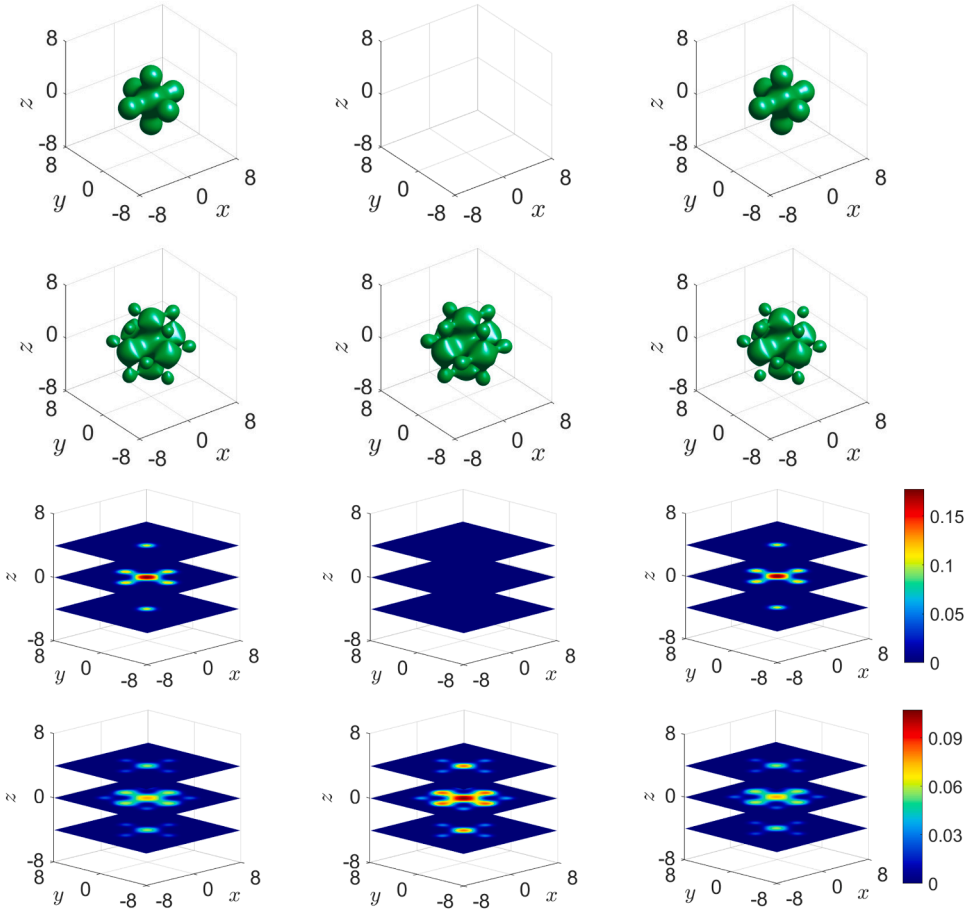

Fig. 5. Isosurface plots and corresponding slice views for the wave functions of the ground state in Example 6. **Case I**: $|\phi_1(x, y, z)| = 0.01$ (left), $|\phi_0(x, y, z)| \equiv 0$ (middle) and $|\phi_{-1}(x, y, z)| = 0.01$ (right) (1st row) with the slice view (3rd row). **Case II**: $|\phi_1(x, y, z)| = 0.01$ (left), $|\phi_0(x, y, z)| = 0.01$ (middle) and $|\phi_{-1}(x, y, z)| = 0.01$ (right) (2nd row) with the slice view (4th row).

Example 4 (1D Case). We study the 1D ground states with $\varepsilon = \frac{1}{\sqrt{50}}$ for both anti-ferromagnetic (**Case I**) and ferromagnetic (**Case II**), whose corresponding parameter details are specified in Example 3.

In our computation, the computational domain is taken as $\Omega = [-16, 16]$. Fig. 2 shows the density of the ground state solutions for two cases. The energy and chemical potential are computed as $E_g = 25.4681$, $\mu_g = 39.1845$ in **Case I**; $E_g = 52.8612$, $\mu_g = 84.7055$ in **Case II**.

Example 5 (2D Case). We study the 2D ground states with $\varepsilon = \frac{1}{\sqrt{20}}$ and two different potentials, i.e, the optical lattice potential Eq. (4.3) and the harmonic + honeycomb potential [8] defined as:

$$V(\mathbf{x}) = \frac{1}{2}(x^2 + y^2) + \beta_0 \left[\cos(\mathbf{b_1} \cdot \mathbf{x}) + \cos(\mathbf{b_2} \cdot \mathbf{x}) + \cos((\mathbf{b_1} + \mathbf{b_2}) \cdot \mathbf{x})\right],$$

with $\mathbf{b_1} = \frac{\pi}{4}(\sqrt{3}, 1), \mathbf{b_2} = \frac{\pi}{4}(-\sqrt{3}, 1)$ and β_0 a tunable constant, for both anti-ferromagnetic (**Case I**) and ferromagnetic (**Case II**), whose corresponding parameter details are specified in Example 2.

In our computation, the computational domain is taken as $\Omega = [-16, 16]^2$. Figs. 3-4 show the density of the ground state solutions for two cases. We compute the energy and chemical potential for the optical lattice potential as $E_g = 11.8976$, $\mu_g = 14.9370$ in **Case I**; $E_g = 16.8160$, $\mu_g = 21.3889$ in **Case II**, and for the Harmonic + honeycomb potential as $E_g = 1.4263$, $\mu_g = 3.8406$ ($\beta_0 = 5$), $E_g = -39.7288$, $\mu_g = -34.7968$ ($\beta_0 = 40$) in **Case I**; $E_g = 6.1017$, $\mu_g = 11.0848$ ($\beta_0 = 5$), $E_g = -31.6668$, $\mu_g = -24.0668$ ($\beta_0 = 40$) in **Case II**.

Example 6 (3D Case). We study the 3D ground states for both anti-ferromagnetic (**Case I**) and ferromagnetic (**Case II**), whose corresponding parameter details are specified in Example 1.

In our computation, the computational domain is taken as $\Omega = [-8, 8]^3$. Fig. 5 shows the profiles of the ground state solutions for two cases. The energy and chemical potential are computed as $E_g = 13.1852$, $\mu_g = 15.6923$ in **Case I**; $E_g = 17.0860$, $\mu_g = 20.5723$ in **Case II**.

5. Conclusion

Starting from the 3D Schrödinger equations with DDI under a strongly anisotropic external potential, we performed a dimension reduction analysis and derived the mean-field GPEs for the quasi-1D and quasi-2D spin-1 dipolar BECs. The PGF algorithm is integrated with KTM, which is utilized for fast and accurate evaluation of dipolar potential, to compute the ground states. For better accuracy and efficiency, we discretized the PGF by treating the Lagrange multiplier term explicitly. Besides the mass constraint, we proposed the other two projection conditions so to determine all the three projection constants uniquely. Convergence results of the dimension reduction were verified in terms of the ground states for the 3D to quasi-2D and 3D to quasi-1D nonlocal GPEs. Extensive numerical results from 1D to 3D in various cases were reported to showcase the efficiency and accuracy. Methods proposed here can be easily extended to complicated spin-F or spin-orbit-coupled dipolar BECs.

CRediT authorship contribution statement

Zhixuan Li: Writing – review & editing, Writing – original draft, Visualization, Methodology, Formal analysis, Data curation; **Qinglin Tang:** Writing – review & editing, Supervision, Project administration, Methodology, Funding acquisition, Formal analysis, Conceptualization; **Hanquan Wang:** Writing – review & editing, Validation, Methodology; **Yong Zhang:** Writing – review & editing, Supervision, Project administration, Methodology, Funding acquisition, Formal analysis, Conceptualization.

Data availability

No data was used for the research described in the article.

Declaration of competing interest

The authors declare the following financial interests/personal relationships which may be considered as potential competing interests.

Acknowledgement

This work was partially supported by the National Key R&D Program of China No. 2024YFA1012803, the National Natural Science Foundation of China No. 12271400 (Z. Li and Y. Zhang), No. 11971335 (Q. Tang), No. 11871418 and 12461081 (H. Wang), and the Institutional Research Fund from Sichuan University No. 2020SCUNL110 (Q. Tang).

Appendix A. Convolution identity

Theorem 1. *Given convolution kernel* $U_{\mathbf{nm}}(\mathbf{x}) = \frac{3}{4\pi}\frac{1}{|\mathbf{x}|^3}\left((\mathbf{n}\cdot\mathbf{m}) - 3\frac{(\mathbf{x}\cdot\mathbf{n})(\mathbf{x}\cdot\mathbf{m})}{|\mathbf{x}|^2}\right)$ *with* $\mathbf{n},\mathbf{m}\in\mathbb{R}^3$ *being unit vectors, for any compact-supported smooth function* $f(\mathbf{x})\in C_c^\infty(\mathbb{R}^3)$*, we have*

$$\left[U_{\mathbf{nm}} * f\right](\mathbf{x}) = -(\mathbf{n}\cdot\mathbf{m})f(\mathbf{x}) - 3\left[\left(\frac{1}{4\pi|\mathbf{x}|}\right) * \partial_{\mathbf{nm}} f\right](\mathbf{x}). \tag{A.1}$$

Proof. Let

$$u(\mathbf{x}) = -3\partial_{\mathbf{nm}}\left(\frac{1}{4\pi|\mathbf{x}|}\right). \tag{A.2}$$

For any fixed $\varepsilon>0$, let $B_\varepsilon = \{\mathbf{x}\in\mathbb{R}^3 | |\mathbf{x}|<\varepsilon\}$ and $B_\varepsilon^c = \{\mathbf{x}\in\mathbb{R}^3 | |\mathbf{x}|\geq\varepsilon\}$. It is straightforward to check that

$$U_{\mathbf{nm}}(\mathbf{x}) = u(\mathbf{x}), \quad 0\neq\mathbf{x}\in\mathbb{R}^3. \tag{A.3}$$

Using Gauss-Green theorem and noticing Eq. (A.3), we get

$$\begin{aligned}
-\frac{1}{3}\int_{B_\varepsilon^c} U_{\mathbf{nm}}(\mathbf{x})f(\mathbf{x})\mathrm{d}\mathbf{x} &= -\frac{1}{3}\int_{B_\varepsilon^c} u(\mathbf{x})f(\mathbf{x})\mathrm{d}\mathbf{x} = \int_{B_\varepsilon^c}\partial_{\mathbf{nm}}\left(\frac{1}{4\pi|\mathbf{x}|}\right)f(\mathbf{x})\mathrm{d}\mathbf{x}\\
&= \int_{B_\varepsilon^c}\left[\partial_{\mathbf{n}}\left(\partial_{\mathbf{m}}\left(\frac{1}{4\pi|\mathbf{x}|}\right)f(\mathbf{x})\right) - \partial_{\mathbf{m}}\left(\frac{1}{4\pi|\mathbf{x}|}\right)\partial_{\mathbf{n}}f\right]\mathrm{d}\mathbf{x}\\
&= -\int_{\partial B_\varepsilon}\partial_{\mathbf{m}}\left(\frac{1}{4\pi|\mathbf{x}|}\right)f(\mathbf{x})\frac{\mathbf{x}\cdot\mathbf{n}}{|\mathbf{x}|}\mathrm{d}S - \int_{B_\varepsilon^c}\left[\partial_{\mathbf{m}}\left(\frac{1}{4\pi|\mathbf{x}|}\right)\partial_{\mathbf{n}}f\right]\mathrm{d}\mathbf{x}\\
&= I_1^\varepsilon - \int_{B_\varepsilon^c}\left[\partial_{\mathbf{m}}\left(\frac{1}{4\pi|\mathbf{x}|}\partial_{\mathbf{n}}f\right) - \frac{1}{4\pi|\mathbf{x}|}\partial_{\mathbf{mn}}f\right]\mathrm{d}\mathbf{x}\\
&= I_1^\varepsilon + I_2^\varepsilon + \int_{B_\varepsilon^c}\frac{1}{4\pi|\mathbf{x}|}\left(\partial_{\mathbf{mn}}f\right)\mathrm{d}\mathbf{x},
\end{aligned} \tag{A.4}$$

where

$$I_1^\varepsilon := -\int_{\partial B_\varepsilon}\partial_{\mathbf{m}}\left(\frac{1}{4\pi|\mathbf{x}|}\right)f(\mathbf{x})\frac{\mathbf{x}\cdot\mathbf{n}}{|\mathbf{x}|}\mathrm{d}S, \quad I_2^\varepsilon := \int_{\partial B_\varepsilon}\frac{1}{4\pi|\mathbf{x}|}\left(\partial_{\mathbf{n}}f\right)\frac{\mathbf{x}\cdot\mathbf{m}}{|\mathbf{x}|}\mathrm{d}S. \tag{A.5}$$

From Eq. (A.5), we get

$$\begin{aligned}
I_1^\varepsilon &= \frac{1}{4\pi\varepsilon^2}\int_{\partial B_\varepsilon}\frac{(\mathbf{x}\cdot\mathbf{m})(\mathbf{x}\cdot\mathbf{n})}{|\mathbf{x}|^2}f(\mathbf{x})\mathrm{d}S\\
&= \frac{1}{4\pi\varepsilon^2}\int_{\partial B_\varepsilon}\frac{(\mathbf{x}\cdot\mathbf{m})(\mathbf{x}\cdot\mathbf{n})}{|\mathbf{x}|^2}f(\mathbf{0})\mathrm{d}S + \frac{1}{4\pi\varepsilon^2}\int_{\partial B_\varepsilon}\frac{(\mathbf{x}\cdot\mathbf{m})(\mathbf{x}\cdot\mathbf{n})}{|\mathbf{x}|^2}[f(\mathbf{x})-f(\mathbf{0})]\mathrm{d}S.
\end{aligned} \tag{A.6}$$

By symmetry, we obtain

$$\begin{aligned}
\int_{\partial B_\varepsilon}\frac{(\mathbf{x}\cdot\mathbf{m})(\mathbf{x}\cdot\mathbf{n})}{|\mathbf{x}|^2}\mathrm{d}S &= \int_{\partial B_\varepsilon}\frac{\mathrm{n}_1\mathrm{m}_1\mathrm{x}^2+\mathrm{n}_2\mathrm{m}_2\mathrm{y}^2+\mathrm{n}_3\mathrm{m}_3\mathrm{z}^2}{|\mathbf{x}|^2}\mathrm{d}S\\
&= \int_{\partial B_\varepsilon}\frac{\frac{1}{3}(\mathrm{n}_1\mathrm{m}_1|\mathbf{x}|^2+\mathrm{n}_2\mathrm{m}_2|\mathbf{x}|^2+\mathrm{n}_3\mathrm{m}_3|\mathbf{x}|^2)}{|\mathbf{x}|^2}\mathrm{d}S\\
&= \int_{\partial B_\varepsilon}\frac{(\mathbf{n},\mathbf{m})|\mathbf{x}|^2}{3|\mathbf{x}|^2}\mathrm{d}S = 4\pi\varepsilon^2\frac{(\mathbf{n},\mathbf{m})}{3},
\end{aligned} \tag{A.7}$$

$$\begin{aligned}
\left|\int_{\partial B_\varepsilon}\frac{(\mathbf{x}\cdot\mathbf{m})(\mathbf{x}\cdot\mathbf{n})}{|\mathbf{x}|^2}[f(\mathbf{x})-f(\mathbf{0})]\mathrm{d}S\right| &= \left|\int_{\partial B_\varepsilon}\frac{(\mathbf{x}\cdot\mathbf{m})(\mathbf{x}\cdot\mathbf{n})}{|\mathbf{x}|^2}[\mathbf{x}\cdot\nabla f(\theta\mathbf{x})]\mathrm{d}S\right|\\
&\leq \varepsilon\|\nabla f\|_{L^\infty(B_\varepsilon)}\int_{\partial B_\varepsilon}\mathrm{d}S = 4\pi\varepsilon^3\|\nabla f\|_{L^\infty(B_\varepsilon)},
\end{aligned} \tag{A.8}$$

where $1\leq\theta\leq 1$, plugging Eqs. (A.7) and (A.8) into (A.6), we have

$$I_1^\varepsilon \to \frac{1}{3}f(\mathbf{0})(\mathbf{n},\mathbf{m}), \quad \boldsymbol{\varepsilon}\to\mathbf{0}^+. \tag{A.9}$$

Similarly, for $\varepsilon\to 0^+$, we get

$$\left|I_2^\varepsilon\right| \leq \|\nabla f\|_{L^\infty(B_\varepsilon)}\int_{\partial B_\varepsilon}\frac{1}{4\pi\varepsilon}\mathrm{d}S = \varepsilon\|\nabla f\|_{L^\infty(B_\varepsilon)}\to 0. \tag{A.10}$$

Combining Eqs. (A.9) and (A.10), taking $\varepsilon\to 0^+$ in Eq. (A.4), we obtain

$$\int_{\mathbb{R}^3} U_{\mathbf{nm}}(\mathbf{x})f(\mathbf{x})\mathrm{d}\mathbf{x} = -(\mathbf{n},\mathbf{m})f(\mathbf{0}) - 3\int_{\mathbb{R}^3}\left(\frac{1}{4\pi|\mathbf{x}|}\right)\partial_{\mathbf{nm}}f(\mathbf{x})\mathrm{d}\mathbf{x}. \tag{A.11}$$

Furthermore, defining $f_{\mathbf{y}}(\mathbf{x}) := f(\mathbf{y}-\mathbf{x})$, $\forall \mathbf{y} \in \mathbb{R}^3$ and plugging into Eq. (A.11), we have

$$\left[U_{\mathbf{nm}} * f\right](\mathbf{x}) = -(\mathbf{n}\cdot\mathbf{m}) f(\mathbf{x}) - 3\left[\left(\frac{1}{4\pi|\mathbf{x}|}\right) * \partial_{\mathbf{nm}} f\right](\mathbf{x}). \tag{A.12}$$

□

Appendix B. The projection coefficients

In order to find the other two projections or normalization equations used in the projection step, we first generalize the gradient flow with discrete normalization (GFDN) for computing the ground state of the spin $F=1$ dipolar BECs, from $t_n \le t < t_{n+1}, n \ge 1$:

$$\partial_t \Phi(\mathbf{x},t) = \left[\frac{1}{2}\nabla^2 - V(\mathbf{x}) - \lambda_n \rho - \lambda_s \mathbf{F}\cdot\mathbf{f} - \lambda_d \mathbf{D}\cdot\mathbf{f}\right]\Phi, \tag{B.1}$$

followed by a projection step as

$$\phi_j(\mathbf{x},t_{n+1}) := \phi_j(\mathbf{x},t_{n+1}^+) = \sigma_j^n \phi_j(\mathbf{x},t_{n+1}^-), \quad \mathbf{x}\in\Omega, \quad j=1,0,-1, \tag{B.2}$$

where $\phi_j(\mathbf{x},t_{n+1}^{\pm}) = \lim_{t\to t_{n+1}^{\pm}} \phi_j(\mathbf{x},t)$ and σ_j^n are projection constants which are chosen such that $\|\Phi(\cdot,t_{n+1})\|^2 = \sum_{j=-1}^{1} \|\phi_j(\cdot,t_{n+1})\|^2 = 1$. The normalized gradient flow Eqs. (B.1)–(B.2) can be viewed as applying a time-splitting scheme to the PGF Eq. (3.1) and the projection step Eq. (B.2) is equivalent to solving the following nonlinear ordinary differential equations:

$$\partial_t \phi_j(\mathbf{x},t) = \mu_\Phi(t)\,\phi_j, \quad t_n \le t \le t_{n+1}, \quad n \ge 0.$$

The solution of the above ODEs can be expressed as

$$\phi_j(\mathbf{x},t_{n+1}) = \exp\left(\int_{t_n}^{t_{n+1}} \mu_\Phi(\tau)\mathrm{d}\tau\right)\phi_j(\mathbf{x},t_n), \quad j=1,0,-1.$$

This immediately suggests the projection parameters satisfy

$$\sigma_1^n = \sigma_0^n = \sigma_{-1}^n.$$

References

[1] M. H. Anderson, J. R. Ensher, M. R. Matthewa, C. E. Wieman, E. A. Cornell, Observation of Bose-Einstein condensation in a dilute atomic vapor, Science 269 (1995) 198–201.
[2] X. Antoine, A. Levitt, Q. Tang, Efficient spectral computation of the stationary states of rotating Bose-Einstein condensates by the preconditioned nonlinear conjugate gradient method, J. Comput. Phys. 343 (2017) 92–109.
[3] X. Antoine, Q. Tang, Y. Zhang, A preconditioned conjugated gradient method for computing ground states of rotating dipolar Bose-Einstein condensates via kernel truncation method for dipole-dipole interaction evaluation, Commun. Comput. Phys. 24 (2018) 966–988.
[4] X. Antoine, Q. Tang, Y. Zhang, On the ground states and dynamics of space fractional nonlinear Schrödinger/Gross-Pitaevskii equations with rotation term and nonlocal nonlinear interactions, J. Comput. Phys. 325 (2016) 74–97.
[5] W. Bao, I.-L. Chern, F. Lim, Efficient and spectrally accurate numerical methods for computing ground and first excited states in Bose-Einstein condensates, J. Comput. Phys. 219 (2006) 836–854.
[6] W. Bao, I.-L. Chern, Y. Zhang, Efficient numerical methods for computing ground states of spin-1 Bose-Einstein condensates based on their characterizations, J. Comput. Phys. 253 (2013) 189–208.
[7] W. Bao, Q. Du, Computing the ground state solution of Bose-Einstein condensates by a normalized gradient flow, SIAM J. Sci. Comput. 30 (2008) 1925–1948.
[8] W. Bao, H. Jian, N. J. Mauser, Y. Zhang, Dimension reduction of the Schrödinger equation with Coulomb and anisotropic confining potentials, SIAM J. Appl. Math. 6 (2013) 2100–2123.
[9] W. Bao, S. Jiang, Q. Tang, Y. Zhang, Computing the ground state and dynamics of the nonlinear Schrödinger equation with nonlocal interactions via the nonuniform FFT, J. Comput. Phys. 296 (2015) 72–89.
[10] W. Bao, F. Lim, Computing ground states of spin-1 Bose-Einstein condensates by the normalized gradient flow, SIAM J. Sci. Comput. 30 (2008) 1925–1948.
[11] W. Bao, W. Tang, Ground-state solution of Bose-Einstein condensate by directly minimizing the energy functional, J. Comput. Phys. 187 (2003) 230–254.
[12] W. Bao, H. Wang, A mass and magnetization conservative and energy-diminishing numerical method for computing ground state of spin-1 Bose-Einstein condensates, SIAM J. Numer. Anal. 45 (2007) 2177–2200.
[13] M. D. Barrett, J. A. Sauer, M. S. Chapman, All-optical formation of an atomic Bose-Einstein condensate, Phys. Rev. Lett. 87 (2001) 010404.
[14] I. Danaila, P. Kazemi, A new Sobolev gradient method for direct minimization of the Gross-Pitaevskii energy with rotation, SIAM J. Sci. Comput. 32 (2010) 2447–2467.
[15] I. Danaila, B. Protas, Computation of ground states of the Gross-Pitaevskii functional via Riemannian optimization, SIAM J. Sci. Comput. 39 (2017) 1102–1129.
[16] L. Exl, N. J. Mauser, Y. Zhang, Accurate and efficient computation of nonlocal potentials based on Gaussian-sum approximation, J. Comput. Phys. 327 (2016) 629–642.
[17] L. Greengard, S. Jiang, Y. Zhang, The anisotropic truncated kernel method for convolution with free-space Green's functions, SIAM J. Sci. Comput. 40 (2018) 3733–3754.
[18] S. Jiang, L. Greengard, W. Bao, Fast and accurate evaluation of nonlocal Coulomb and dipole-dipole interactions via the nonuniform FFT, SIAM J. Sci. Comput. 36 (2014) 777–794.
[19] Y. Kawaguchi, H. Saito, K. Kudo, M. Ueda, Spontaneous magnetic ordering in a ferromagnetic spinor dipolar Bose-Einstein condensate, Phys. Rev. A 82 (2010) 043627.
[20] Y. Kawaguchi, H. Saito, M. Ueda, Can spinor dipolar effects be served in Bose-Einstein condensates?, Phys. Rev. Lett. 98 (2007) 110406.
[21] Y. Kawaguchi, H. Saito, M. Ueda, Einstein-de Haas effect in dipolar Bose-Einstein condensates, Phys. Rev. Lett. 96 (2006) 080405.
[22] Y. Kawaguchi, H. Saito, M. Ueda, Spontaneous circulation in ground-state spinor dipolar Bose-Einstein condensates, Phys. Rev. Lett. 97 (2006) 130404.
[23] W. Liu, Y. Cai, Normalized gradient flow with Lagrange multiplier for computing ground states of Bose-Einstein condensates, SIAM J. Sci. Comput. 43 (2021) 219–243.
[24] X. Liu, Q. Tang, S. Zhang, Y. Zhang, On optimal zero-padding of kernel truncation method, SIAM J. Sci. Comput. 46 (2024) 23–49.

[25] F. Méhats, Analysis of a quantum subband model for the transport of partially confined charged particles, Monatch. Math. 147 (2006) 43–73.
[26] T. Ohmi, K. Machida, Bose-Einstein condensation with internal degrees of freedom in alkali atom gases, J. Phys. Soc. Jpn. 67 (1998) 1822–1825.
[27] S. E. Pollack, D. Dries, M. Junker, Y. P. Chen, T. A. Corcovilos, R. G. Hulet, Extreme tunability of interactions in a ^{7}Li Bose-Einstein condensate, Phys. Rev. Lett. 102 (2009) 090402.
[28] S. Ronen, D. C. Bortolotti, J. Bohn, Bogoliubov modes of a dipolar condensate in a cylindrical trap, Phys. Rev. A 74 (2006) 013623.
[29] C. A. Rozzi, D. Varsano, A. Marini, E. K. U. Gross, A. Rubio, Exact Coulomb cutoff technique for supercell calculations, Phys. Rev. B 73 (2006) 205119.
[30] Q. Tang, Y. Zhang, N. J. Mauser, A robust and efficient numerical method to compute the dynamics of the rotating two-component dipolar Bose-Einstein condensates, Comput. Phys. Commun. 219 (2017) 223–235.
[31] T. Tian, Y. Cai, X. Wu, Z. Wen, Ground states of spin-F Bose-Einstein condensates, SIAM J. Sci. Comput. 42 (2020) 983–1013.
[32] M. Ueda, Y. Kawaguchi, Spinor Bose-Einstein condensates, Phys. Rep. 520 (2012) 253–381.
[33] F. Vico, L. Greengard, M. Ferrando, Fast convolution with free-space Green's functions, J. Comput. Phys. 323 (2016) 191–203.
[34] H. Wang, A projection gradient method for computing ground state of spin-2 Bose-Einstein condensates, J. Comput. Phys. 274 (2014) 473–488.
[35] X. Wu, Z. Wen, W. Bao, A regularized Newton method for computing ground states of Bose-Einstein condensates, J. Sci. Comput. 73 (2017) 303–329.
[36] S. Yi, H. Pu, Spontaneous spin textures in dipolar spinor condensates, Phys. Rev. Lett. 97 (2006) 020401.
[37] Y. Zhang, Fast evaluation of convolution-type nonlocal potential, Math. Numer. Sin. 45 (2023) 385–400.
[38] Q. Zhuang, J. Shen, Efficient SAV approach for imaginary time gradient flows with applications to one- and multi-component Bose-Einstein condensates, J. Comput. Phys. 396 (2019) 72–88.